HHS Public Access

Author manuscript

Mol Psychiatry. Author manuscript; available in PMC 2020 December 05.

Published in final edited form as:

Mol Psychiatry. 2020 December ; 25(12): 3360–3379. doi:10.1038/s41380-019-0547-5.

UPF2 leads to degradation of dendritically-targeted mRNAs to regulate synaptic plasticity and cognitive function

Michael Notaras[1], **Megan Allen**[1], **Francesco Longo**[2], **Nicole Volk**[1], **Miklos Toth**[3], **Noo Li Jeon**[4], **Eric Klann**[2], **Dilek Colak**[1,5,*]

[1]Center for Neurogenetics, Feil Family Brain and Mind Research Institute, Weill Cornell Medical College, Cornell University, New York City, New York, USA.

[2]Center for Neural Science, New York University, New York City, New York, USA.

[3]Department of Pharmacology, Weill Cornell Medical College, Cornell University, New York City, New York, USA.

[4]School of Mechanical and Aerospace Engineering, Seoul National University, Seoul, South Korea.

[5]Gale & Ira Drukier Institute for Children's Health, Weill Cornell Medical College, Cornell University, New York City, New York, USA.

Abstract

Synaptic plasticity requires a tight control of mRNA levels in dendrites. Consistently, RNA translation and degradation pathways have been recently linked to neurodevelopmental and neuropsychiatric diseases, suggesting a role for RNA regulation in synaptic plasticity and cognition. While the local translation of specific mRNAs has been implicated in synaptic plasticity, the tightly-controlled mechanisms that regulate local quantity of specific mRNAs remains poorly understood. Despite being the only RNA regulatory pathway that is associated with multiple mental illnesses, the Nonsense-Mediated mRNA Decay (NMD) pathway presents an unexplored regulatory mechanism for synaptic function and plasticity. Here, we show that neuron-specific disruption of UPF2, an NMD component, in adulthood attenuates learning, memory, spine density, synaptic plasticity (L-LTP), and potentiates perseverative/repetitive behavior. We report that the NMD pathway operates within dendrites to regulate GLUR1 surface levels. Specifically, UPF2 modulates the internalization of GLUR1 and promotes its local synthesis in dendrites. We identified PRKAG3 as a mechanistic substrate for NMD that contributes to the UPF2-mediated regulation of GLUR1 by limiting total GLUR1 levels. These data establish that UPF2 regulates synaptic plasticity, cognition, and local protein synthesis in dendrites, providing fundamental insight into the neuron-specific function of NMD within the brain.

*Correspondence: dic2009@med.cornell.edu.

Author contributions

M.N. performed and/or analyzed most of the experiments including behavioral assays, and manuscript preparation/writing. M.A. prepared all neuronal cultures. F.L. performed electrophysiology experiments. N.V. provided technical assistance. M.T. provided infrastructure support. N.L.J. designed and manufactured microfluidic devices. E.K. supervised electrophysiology experiments. D.C. initiated and conceived the project; designed, analyzed, and supervised experiments; and wrote the manuscript. All authors contributed to the experimental design and interpretation and commented on the manuscript.

Conflict of Interests

The authors have no known conflict of interests to report.

Introduction

NMD is a process that regulates protein expression through degradation of specific mRNAs [1-3]. NMD was first identified as an mRNA surveillance pathway that degrades mRNAs undergoing premature termination of translation [4-6]. In most mRNAs, all exon-junction complexes (EJCs), a group of proteins bound to mRNA after splicing, are upstream of the termination codon. While Up-Frameshift (UPF) proteins UPF2 and UPF3B are part of the EJC, UPF1 is only recruited to mRNA if an EJC is a downstream of a termination codon, making this codon perceived as premature, and the mRNA considered nonsense. This initiates NMD and ultimately leads to mRNA degradation [7, 8]. Recently, it has been shown that NMD also targets physiological mRNAs that naturally have NMD-inducing features but code for functional proteins [9-12]. For instance, the mRNA of the synaptic plasticity protein ARC is a known target of NMD due to intron splicing in its 3' UTR [13]. ARC is highly expressed in dendrites [14-17] and is required for synaptic plasticity and memory consolidation [18-21]. Similar to *Arc* mRNA, various mRNAs with intron splicing in 3' UTR are localized to dendrites [22] and have been implicated in synaptic plasticity and memory [19, 23-26]. However, the extent to which NMD is physiologically relevant to synaptic plasticity is not clear.

Despite its putative link to many mental disorders including autism and schizophrenia [27-32], whether NMD is relevant to the synaptic pathology and behavioral deficits of these diseases remains unclear. It has been reported that NMD maintains synapse architecture and synaptic vesicle cycle efficacy in drosophila [33]. NMD has also been implicated in epileptogenesis [34]. In addition, a recent study showed that *Upf3b*-null mice exhibit deficits in fear-conditioned learning, supporting a role for NMD in regulating synaptic plasticity and cognition [35]. However, because NMD is ubiquitous and required for neuronal differentiation [36], disruption of this pathway during development hinders determining the direct role of NMD in these processes. Therefore, understanding the precise, cell-type specific role of NMD in developing and adult brain is likely to provide novel insights into key mechanisms critical for synaptic plasticity and behavior.

Synaptic plasticity takes several forms, including the modification of synaptic strength and spine structure. Synaptic transmission can be influenced by activity, becoming either enhanced, through long-term potentiation (LTP), or depressed, through long-term depression (LTD) [37]. Many cognitive disorders are associated with alterations in spine density and synaptic plasticity [38, 39]. Both LTP and LTD has been associated with local protein synthesis in dendrites [21, 40]. Deficits in mRNA regulation can result in ectopic protein synthesis and lead to cognitive disabilities [41-47], having downstream effects on synaptic plasticity and cognition. For example, exaggerated mRNA translation leads to alterations in spine density, LTP and LTD [44, 47-49] suggesting that a tight control of protein synthesis is required at many levels within dendrites [42]. A great amount of prior research has addressed the pathways that regulate translational derepression in dendrites. However, the mechanisms that control mRNA quantity during synaptic function remain unknown.

Here we show that both synaptic plasticity and cognitive function is physiologically regulated by neuronal NMD. Conditional deletion of the NMD gene *Upf2* in adult glutamatergic neurons *in vivo* disrupts learning and memory and potentiates perseverative/repetitive behavior. Deletion of *Upf2* also results in altered spine density and LTP in the adult hippocampus. This phenotype is accompanied by a significant reduction in total GLUR1 levels in conditional knockout mice. We show that UPF2 regulates GLUR1 surface levels through mechanisms that influences GLUR1 internalization and nascent protein synthesis. Selective disruption of UPF2 protein from cultured hippocampal neurons reduces both total and surface expression of GLUR1 protein without affecting *GluR1* mRNA levels. This phenotype is recapitulated when NMD is disrupted in dendrites via the targeted-inhibition of UPF3B local synthesis. Disruption of UPF2 increases internalization, due to elevated ARC levels, and decreases synthesis, due to elevated PRKAG3 levels, of GLUR1 protein in dendrites. Normalizing the levels of *Arc* and *Prkag3* mRNAs, together, completely corrects surface GLUR1 levels in UPF2-deficient dendrites. These data demonstrate a role for NMD in regulating cognitive function, the dendritic proteome, and synaptic plasticity, as well as potentially other essential dendritic functions.

Results

UPF2 is required for learning and memory and suppresses perseverative behavior.

We first sought to determine the requirement for neuronal NMD in cognitive function and synaptic plasticity. To do this, we genetically disrupted NMD in postmitotic glutamatergic neurons using a conditional knockout mouse of *Upf2* (*Upf2*$^{fl/fl}$) [50] [11, 50, 51]. We temporally controlled UPF2 disruption by crossing the *Upf2*$^{fl/fl}$ line with a mouse line that expresses tamoxifen-inducible Cre under the αCaMKII promoter (α*CaMKII*:*CreER*^{T2}) [52]. In all behavioral experiments, we induced Cre in 2-month old conditional-knockout (*Upf2*$^{fl/fl}$;α*CaMKII*:*CreER*$^{T2.}$ CKO) mice as well as in their control littermates (*Upf2*$^{wt/wt}$;α*CaMKII*:*CreER*^{T2}; CTRL) by tamoxifen. Loss of UPF2 protein in excitatory neurons was successfully achieved by 200mg/kg of tamoxifen administered every other day for 5 doses (Figure S1a). No difference in locomotor activity, anxiety-related behavior, or sociability phenotypes, were detected between *Upf2* CKO mice and controls (Figure S1b-e).

We next examined hippocampus-dependent learning and memory in *Upf2* CKO mice. On the Y-maze, *Upf2* CKO mice showed no preference for the novel arm relative to the other arms, and displayed significantly worse novel arm preference than the control group (Figure 1a), suggesting that *Upf2* CKO mice have disrupted short-term spatial memory. As an additional measure of hippocampal function, we tested *Upf2* CKO mice for contextual fear memory. In this test, *Upf2 CKO* mice froze for significantly less time than controls by the last tone-shock pairing during conditioning, and this conditioning deficit resulted in worse contextual fear memory in *Upf2* CKO mice relative to control mice 24 hr later (Figure 1b-c). In the Morris water maze, *Upf2* CKO mice displayed a 1) robust attenuation of learning behavior, 2) increased latencies to enter the hidden platform quadrant during the probe trial, and 3) decreased exploration of this quadrant during probe testing (Figure 1d-f). These data collectively suggest that *Upf2* CKO mice exhibit attenuated learning behavior, which

produces worse performance on common assays of hippocampus-dependent memory function.

Because the NMD pathway has been previously linked to autism and schizophrenia [27-32], where stereotypies are common to both disorders, we also tested for perseverative/repetitive behaviors [47, 53-56]. In our marble burying assay, *Upf2* CKO mice buried significantly more marbles than control mice (Figure 1g; 81.14% vs 58.86% of marbles). In an activity-sampling test session, where grooming behavior was continuously monitored for 20 min, CKO mice groomed for longer and displayed a greater frequency of grooming bouts compared to the control group (Figure 1h-i). Together, these data suggest that NMD is required for proper learning and memory, and its disruption potentiates perseverative/repetitive behaviors.

UPF2 ensures proper spine density and L-LTP in hippocampus.

To study spine density in *Upf2* CKO mice, we injected AAV-αCaMKII-eGFP virus into the dorsal CA1 field 7d prior to perfusion. We observed significantly reduced CA1 spine density in *Upf2* CKO hippocampal dendrites compared to control dendrites *in vivo* (Figure 1j). We next assessed both LTD, early phase LTP (E-LTP), and late phase LTP (L-LTP), in these mice. LTD was not different in UPF2-deficient slices compared to control slices (Figure S1f-g), Similarly, we found that E-LTP, which is thought not to require new gene transcription or mRNA translation, was unaltered in UPF2-deficient slices. However, we found that L-LTP, which requires new gene transcription, translation, and AMPA-receptor increase, was significantly decreased in UPF2-deficient slices compared to control slices (Figure 1k-l). These data suggest that NMD is required for proper LTP and spine density but not for LTD in hippocampus.

UPF2 positively regulates GLUR1 surface expression.

We next sought to identify mechanisms through which NMD regulates synaptic plasticity and cognitive function. It was previously shown that disruption of the EJC, a critical component for targeting mRNAs to the NMD pathway, causes an increase in the levels of AMPA receptor GLUR1 in hippocampal dendrites *in vitro* [13]. However, EJC proteins have multiple other functions, including mRNA transport and translation [57]. For example, genetic screens in drosophila showed that knockdown of EJC core components caused skipping of several exons in pre-mRNAs, which contain long introns [58]. Therefore, disruption of EJC might lead to differential phenotypes that are divergent from what occurs when the NMD machinery is discretely targeted. Intriguingly, contrary to what is observed in studies of disrupted EJC proteins, we found that UPF2 deficiency led to a decrease in total GLUR1 levels *in vivo* (Figure 1m). Additionally, this data is congruent with disrupted hippocampal LTP in *Upf2* CKO mice given that LTP can be represented by the synaptic insertion of AMPA receptors [59]. To explore this phenotype *in vitro*, we infected hippocampal neurons with *Upf2*-shRNA:GFP lentivirus to interrupt endogenous NMD activity at 7 days *in vitro* (DIV7) and examined GLUR1 expression on DIV21. Using 2 unique *Upf2*-shRNA lentiviruses (Figure S2), we found that total levels of GLUR1 were decreased both in cell bodies and dendrites of hippocampal neurons upon knockdown of *Upf2* (Figure S3a-c).

We next asked whether UPF2 regulates GLUR1 surface expression in neurons. An essential component of GLUR1 signaling involves the dynamic insertion and removal of the GLUR1 receptor to the synaptic surface [60]. Similar to total GLUR1 levels, UPF2 deficiency led to decreased surface levels of GLUR1 (Figure 2; see also Figure S3 and S4). This suggests that NMD positively regulates GLUR1 surface expression. While *GluR1* mRNA is not a canonical target of NMD, it is known that some mRNAs that do not carry identifiable NMD-inducing features can also be degraded by NMD [61]. In addition, it has been suggested that *GluR1* transcription is regulated by ARC [62]. Consistent with *Arc* mRNA being an established target of NMD [11, 13, 63-67] (see also Figure S5), the levels of both *Arc* mRNA and ARC protein are increased in hippocampal neurons upon knockdown of *Upf2* (Figure S5). We, therefore, examined *GluR1* mRNA levels in UPF2-deficient neurons. Overall *GluR1* mRNA levels were unaltered following knockdown of *Upf2* in hippocampal neurons, indicating that the reduction in total and surface GLUR1 protein does not arise from changes in mRNA availability. These data thus suggest that NMD modulates GLUR1 signaling via an indirect restraining mechanism that negatively regulates the synthesis, surface localization or surface turnover of GLUR1 in dendrites.

UPF2 negatively regulates GLUR1 internalization in dendrites.

We next sought to determine how UPF2 regulates surface expression of GLUR1 in dendrites. It is possible that the reduction in total GLUR1 levels might account for decreased surface levels of this receptor. However, locally synthesized ARC is also known to cause GLUR1 endocytosis, leading to a decrease in the surface levels of this receptor [21, 68]. To determine if GLUR1 endocytosis is altered after disruption of NMD, we measured the basal internalization rate of GLUR1 upon knockdown of *Upf2* in hippocampal dendrites using a previously established protocol [69]. We observed significantly increased GLUR1 basal internalization in UPF2-deficient dendrites (Figure 3a-b). However, ARC-mediated internalization of GLUR1 only influences surface but not total levels of GLUR1 [70], indicating that UPF2 must regulate total GLUR1 levels via other, yet defined, NMD targets.

UPF2 positively regulates local synthesis of GLUR1 in dendrites.

The total levels of dendritic GLUR1 are determined by the amount of GLUR1 protein trafficked to dendrites from cell bodies as well as a balance of local protein synthesis [71] and local protein degradation [72, 73] in dendrites. Thus, we also investigated the possibility of enhanced GLUR1 proteolysis or decreased GLUR1 synthesis in UPF2-deficient dendrites. To do this, we used a custom-fabricated tripartite microfluidic device, which, unlike traditional microfluidic chambers with two channels [74], contains a third “synaptic” channel (Figure 3c and Figure S6-7). This tripartite compartmentalization creates physical and fluidic isolation of presynaptic neurons, postsynaptic neurons, and their synapsing projections, enabling us to selectively isolate, treat and harvest dendrites in subsequent experiments.

When AMPA receptors are internalized, endocytosed receptors undergo lysosome- or proteasome-mediated degradation [73, 75-78]. To study local degradation of GLUR1, we cultured E16 hippocampal neurons in tripartite chambers and applied control- or *Upf2*-shRNA viruses only to postsynaptic cell channels at DIV7. This resulted in disruption of

NMD only in postsynaptic cell bodies and dendrites but not in presynaptic cells (Figure S7). At DIV21, we inhibited both proteosomal and lysosomal degradation by treating the synaptic channels with MG132 and leupeptin. Co-inhibition of lysosome- and proteasome-mediated degradation did not restore GLUR1 levels in UPF2-deficient dendrites (Figure S8). Thus, degradation of GLUR1 receptors at the protein-level does not contribute to the reduction in surface GLUR1 observed in UPF2-deficient dendrites.

We next asked whether local synthesis of the GLUR1 receptor is altered in UPF2-deficient dendrites. To measure the dendritic synthesis of GLUR1, we used a CLICK-chemistry based approach and labeled locally synthesized nascent proteins at synapses (Figure 3c-e). We cultured E16 hippocampal neurons in tripartite chambers and targeted NMD only in postsynaptic cells by applying the *Upf2*-shRNA virus into the postsynaptic cell channel at DIV7. At DIV21, we exchanged the growth medium in the synaptic channels to methionine-free medium containing the methionine analog azidohomoalanine (AHA) [79] to label all newly synthesized proteins at synapses (Figure 3d). The amount of GLUR1 protein that bound the streptavidin in the UPF2-deficient synapses was significantly lower compared to the amount of GLUR1 that bound the streptavidin in the control synapses (Figure 3e). This data suggests that dendritic synthesis of GLUR1 is reduced upon disruption of NMD.

Local degradation of *Arc* and *Prkag3* mRNAs by NMD in dendrites.

We next sought to determine whether local NMD contributes to the regulation of GLUR1 protein synthesis in dendrites. Similar to *Arc* mRNA, the mRNA of PRKAG3 protein, the non-catalytic subunit of AMP-activated protein kinase (AMPK), is also derived from removal of a 3'UTR intron [13] making the *Prkag3* mRNA a potential substrate for NMD. Indeed, the half-life and mRNA/pre-mRNA ratio of *Prkag3* is increased upon loss of UPF2 in hippocampal neurons (Figure S5). Interestingly, AMPK has been suggested to negatively regulate GLUR1 protein levels in dendrites in a translation dependent manner [25]. Intriguingly, both *Arc* and *Prkag3* mRNAs are localized to dendrites, suggesting that they might be degraded by NMD in these compartments.

We found that the core proteins of the NMD machinery are localized to dendrites (Figure 4a), suggesting that local NMD might contribute to regulation of GLUR1 levels in these compartments. We first examined *Arc* and *Prkag3* mRNA levels in UPF2-deficient synaptic regions. To do this, at DIV7, we selectively infected postsynaptic neurons with *Upf2*-shRNA lentivirus and isolated RNA from synaptic channels at DIV21. qRT-PCR showed an increase in the levels of both *Arc* and *Prkag3* mRNAs in UPF2-deficient synaptic channels compared to control synaptic channels (Figure 4b). NMD is initiated when UPF1 recognizes NMD-inducing features in mRNAs during translation [80, 81]. Thus, inhibition of translation hinders NMD and leads to the accumulation of NMD-target mRNAs [7]. To confirm whether *Arc* and *Prkag3* undergo translation-dependent degradation in synaptic regions, we cultured E16 neurons in tripartite chambers and, at DIV21, applied translation inhibitor cycloheximide (CHX) selectively to synaptic channels. qRT-PCR on harvested synaptic-channel material revealed that both *Arc* and *Prkag3* mRNAs accumulated in these compartments upon inhibition of translation (Figure 4c).

We next asked whether NMD contributes to the regulation of GLUR1 surface levels locally in dendrites. To address this, we inhibited the local synthesis of UPF3B, a protein specific to the NMD pathway [82, 83], selectively in synaptic channels. The local translation of *Upf3b* mRNA is a source for UPF3B protein in dendrites (Figure S9a-b). We cultured E16 neurons in cell-body channels and, starting at DIV14, repeatedly treated synaptic channels with siRNAs against *Upf3b* mRNA for seven days. This resulted in complete loss of UPF3B protein in synaptic channels (Figure S9d). Similar to the knockdown of *Upf2* in postsynaptic cells, the surface frequency of GLUR1 was reduced upon selective loss of UPF3B protein in synaptic channels (Figure 4d).

Taken together, these experiments establish the local requirement for NMD in synaptic regions and that the local regulation of GLUR1 by NMD might, in addition to degrading *Arc*, also involve *Prkag3* degradation.

PRKAG3 negatively regulates GLUR1 expression in dendrites.

We next examined whether PRKAG3 protein locally influences GLUR1 expression in synaptic channels. To do this, we cultured E16 neurons in cell-body channels and, starting at DIV14, repeatedly treated synaptic channels with siRNAs against the *Prkag3* mRNA for seven days (Figure S9e). Selective loss of PRKAG3 in synaptic channels significantly increased the total levels of GLUR1 (Figure 4e).

Because the synaptic channels of tripartite chambers contain both dendrites and axons, it is possible that GLUR1 phenotypes may arise also from axonal changes and therefore not selectively from dendrites. To clarify this, we examined the proteins of the NMD machinery and targets of NMD in mature axons. Neither the components of the NMD machinery, nor *Arc* or *Prkag3* mRNAs, were present in isolated hippocampal axons at DIV21 (Figure S10). In fact, the axonal transcriptome significantly shrinks as axons mature [84] and does not include any known NMD targets [85, 86]. These data indicate that alterations in GLUR1 expression upon selective disruption of either UPF3B or PRKAG3 proteins in synaptic channels therefore solely originate from a local effect within dendrites.

Normalization of *Prkag3* and *Arc* mRNA levels rescues GLUR1 surface expression and spine density in UPF2-deficient dendrites.

We functionally tested a mechanistic role of locally synthesized ARC and PRKAG3 in the NMD-mediated regulation of surface GLUR1 expression. To do this, we systematically modulated the elevated levels of *Arc* and *Prkag3* mRNAs in UPF2-deficient dendrites by siRNA transfection of synaptic channels. We first determined the concentration of siRNA required to correct *Arc* and *Prkag3* levels in UPF2-deficient dendrites (Figure S11). Using optimized concentrations, we next modulated the levels of *Arc* and *Prkag3* mRNAs in synaptic channels containing UPF2-deficient dendrites (Figure 5a). Compared to synaptic channels with intact NMD, cultures infected with *Upf2*-shRNA lentivirus had significantly lower GLUR1 density as expected. Restoring expression levels of *Arc* or *Prkag3* mRNAs in synaptic channels led to a significant but incomplete recovery of surface GLUR1 in these compartments for each target (Figure 5b-c). This is consistent with observations that targeting *Arc* only rescues the internalization of GLUR1, while normalization of *Prkag3*

only rescues total GLUR1 levels but not the increased rates of internalization (Figure S12). Thus, we reinstated both *Arc* and *Prkag3* mRNA levels together, which led to a complete recovery of surface GLUR1 density in UPF2-deficient dendrites (Figure 5b-c). To test this mechanism *in vivo*, we next sought to rescue spine density, which is dependent upon a 3D environment and not readily testable *in vitro*. To normalize *Arc* and *Prkag3* levels *in vivo*, we infected CA1 hippocampal neurons of *Upf2* CKO mice with lentiviruses expressing shRNAs against *Arc* and *Prkag3*. We used shRNA sequences that sufficiently modulated the increased levels of ARC and PRKAG3 proteins in UPF2-deficient neurons (Figure S13). The simultaneous modulation of *Arc* and *Prkag3* in *Upf2* CKO hippocampal neurons increased spine density *in vivo* to levels consistent with CTRL mice (Figure 5f). Together, these data indicate a functional role for UPF2-mediated modulation of ARC and PRKAG3 levels within dendrites, which together function to regulate GLUR1 signaling and synaptic plasticity.

Discussion

Our study identifies neuronal NMD as a mechanism that contributes to the regulation of synaptic plasticity and cognitive function. Specifically, we report that NMD influences synaptic plasticity as well as learning and memory. In addition, our data suggests that local NMD participates in GLUR1 regulation by limiting ARC and PRKAG3 protein expression in dendrites.

UPF2 regulates synaptic plasticity and cognitive function.

Our data indicate that proper synaptic plasticity and cognitive function requires UPF2. Our data show that UPF2-deficient hippocampal slices show decreased L-LTP. In addition, spine density in the hippocampus of conditional *Upf2* mutant mice is reduced relative to control mice. Mice also show attenuated learning and memory upon conditional ablation of *Upf2* in excitatory neurons. Memory deficits were readily detectable in UPF2-deficient mice on three independent hippocampus-dependent behavioral assays. In addition to attenuated learning and memory, loss of UPF2 in excitatory neurons resulted in perseverative behavior in mice. Together, these data implicate a role for NMD in both synaptic plasticity and behavioral endophenotypes common to a spectrum of neurodevelopmental diseases including autism and schizophrenia.

Our data also provide comprehensive insight into the neuron-specific and spatiotemporal requirement for UPF2 in plasticity and behavior. Recently, a *Upf3b* null mutant mouse line was shown to have fear-conditioning defects but, unlike our observations in *Upf2* CKO mice, no spatial learning deficit [35]. There may be several reasons for this. For instance, NMD is ubiquitous and required for neuronal differentiation [36, 87]. Consistent with this, global interruption of NMD by ablation of *Upf3b* during brain development alters neuronal maturation and is thereby likely to contribute to the behavioral phenotypes observed in the *Upf3b* null mouse line. In addition, while UPF2 and UPF3 proteins are known to be specific to the NMD machinery, it has been suggested that NMD might have different branches in which NMD exerts its function independent of UPF2 or UPF3B [83, 88, 89]. Therefore, studies of conditional *Upf2* deletion provide a platform to dissect not only the temporal and

cell-type specific functions of the NMD machinery, but also branch-specific functions of NMD in brain development and behavior.

UPF2-mediated GLUR1 regulation and its contribution to behavior.

Our data also demonstrate that UPF2 positively regulates GLUR1 signaling in hippocampus. We report that loss of UPF2 protein in adult hippocampal neurons caused a concomitant decrease in total and surface levels of this receptor. Our CLICK-chemistry experiments suggest that UPF2 positively regulates GLUR1 protein synthesis, whereby GLUR1 synthesis in dendrites is repressed in the absence of UPF2 protein leading to reduced local GLUR1 protein. Similarly, we confirm that the mRNA of the AMPK γ subunit (PRKAG3) is a substrate of NMD (Figure 4, S5, and S12). Our data suggests that disruption of PRKAG3 within dendrites increases GLUR1 levels (Figure 4). Activated AMPK is known to interrupt translation by either inhibiting mTOR kinase phosphorylation or the translation elongation factor 2 [90-95]. Consistent with this, upon knockdown of *Upf2* we observed an increase in phosphorylated mTOR, which was rescued when PRKAG3 levels were modulated in these neurons (Figure S14). This modulation also restored total GLUR1 levels in UPF2-deficient dendrites. These data suggest that AMPK represses GLUR1 synthesis, and that NMD limits the amount of the AMPK γ subunit thereby serving as a balance in regulating total levels of the GLUR1 receptor. In addition, loss of UPF2 results in a higher GLUR1 internalization rate. ARC protein induces GLUR1 endocytosis, leading to a decrease in the surface levels of this receptor [21, 68]. Indeed, modulation of ARC levels in UPF2-deficient neurons rescues the GLUR1 internalization phenotype without altering total GLUR1 levels (Figure S12). Therefore, neither ARC modulation nor PRKAG3 modulation alone is capable of restoring the surface expression of GLUR1 upon disruption of UPF2. However, concomitant modulation of both ARC and PRKAG3 protein levels together results in a complete rescue of surface GLUR1 phenotype in UPF2-deficient dendrites (Figure 5). Thus, our data suggests that UPF2-dependent NMD regulates local synthesis and basal rates of GLUR1 internalization by degrading *Prkag3* and *Arc* mRNAs, respectively.

Modulation of AMPA-receptor integrity plays a crucial role in synaptic strength. Strengthening of synapses by LTP or weakening of synaptic strength by LTD can be represented by the synaptic insertion of AMPA receptors [59]. Consistent with this, alterations in GLUR1 levels are linked to impairments in LTP as well as abnormalities in memory [53-55]. Our data explicates that hippocampal L-LTP, which is thought to underlie memory consolidation, is decreased in conditional *Upf2* mutant mice. Activation of glutamate receptors facilitates LTP either by through the enlargement of pre-existing spines or promoting the formation of new spines. Intriguingly, AMPK has been suggested to have negative effects on LTP induction [96]. Therefore, a reduction in spine density is consistent with a decrease in L-LTP in conditional *Upf2* mutants. This phenotype is accompanied by behavioral defects, including a lack of short-term spatial memory in the Y-maze, defective associative fear learning and memory, and attenuated spatial learning and memory on the Morris water maze. Each of these cognitive phenomenon requires activity-dependent synaptic strengthening and/or GLUR1-initiated signaling [53, 97, 98]. Reductions in GLUR1 expression were shown to cause spatial memory dissociations in mice [99]. Contextual conditioning requires not just increased levels of GLUR1, but specifically

surface-localized GLUR1, for task performance [25]. NMD-dependent control of GLUR1 signaling is therefore likely to contribute to the plasticity and behavioral phenotypes *Upf2* CKO mice exhibit. However, we cannot exclude the possibility that NMD regulates other receptors or intracellular signaling pathways that might also contribute to LTP, learning and memory. Induction of either mGluR- or NMDAR-LTD is thought to be associated with reduced spine density. In our electrophysiology experiments we only measured mGluR-based LTD due to our focus on GLUR1, which was not significantly altered in *Upf2* cKO mice. However, we did observe a decrease in spine density, which is often associated with LTD. There are examples that spine density is decreased without an accompanying alteration in mGluR-LTD [100]. Nonetheless, we also cannot rule out alterations in other forms of LTD, such as NMDAR-derived LTD. Although NMDARs are more static than AMPA receptors in mature neurons, subunits of NMDARs are also locally translated in dendrites [101] suggesting that NMD and other dendritically-confined phenomenon may regulate NMDAR dynamics.

Local NMD as a regulator of the dendritic proteome.

We report that NMD can occur locally in dendrites. *Arc* mRNA was shown to be locally degraded in hippocampus [102]. However, the involvement of NMD in this, as well as more broadly hippocampal function, has not been demonstrated. Our data show that the NMD machinery is localized to dendrites, and the levels of the NMD targets *Arc* and *Prkag3* are elevated upon selective inhibition of translation in these compartments (Figure 4c). Local inhibition of dendritic UPF3B synthesis results in reduced surface density of GLUR1, suggesting that the UPF3B-dependent branch of NMD locally influences GLUR1 levels within dendrites.

Our data demonstrate that local translation is regulated by mechanisms that control mRNA degradation in dendrites. NMD is likely to have more targets than *Arc* and *Prkag3* in dendrites. In addition to its canonical targets, NMD may also degrade mRNAs that do not carry identifiable NMD-inducing features [61]. However, the mechanisms by which NMD recognizes its atypical targets remain unclear. This raises the possibility that NMD might be regulating various physiological mRNAs in dendrites that cannot be predicted based on sequence information. Therefore, we cannot exclude the possibility that atypical targets of NMD may also contribute to the NMD-mediated GLUR1 regulation at synapses as well as other synaptic events.

Conclusion.

Our experiments provide fundamental support for the idea that NMD modulates dendritic mRNA availability and therefore synaptic plasticity, learning, and memory. Through a number of locally-confined experiments in microfluidic devices and behavioral/LTP assays in neuron-restricted *UPF2* conditional knockout mice, we define a specific role for the UPF2-dependent NMD pathway in dendrites and synaptic function (see schematic model in Figure S15). Therefore, our paper provides novel insights into basic mechanisms that regulate synaptic function that are also likely to play a role in NMD-implicated diseases such as autism and schizophrenia.

Methods

Mice and constructs

Hippocampal neuronal cultures were prepared from C57BL/6J mouse embryos (Charles River Laboratories). *Upf2*-shRNA 1 virus is on a piLenti-shRNA-GFP backbone carrying one shRNA against the *Upf2* mRNA (AGGCGTATTCTGCACTCTAAAGGCGAGCT). *Upf2*-shRNA 2 virus is on a piLenti-shRNA-GFP backbone carrying four shRNAs against the *Upf2* mRNA (TGAAAGACTATGTTATTTGTTGTATGATA). In experiments with *Upf2* deletion in excitatory neurons, a *Upf2* conditional knockout mouse line, which carries flanked loxP sites in the second exon of this gene, [1] was crossed with α*CaMKII*:*CreER*^{T2} line [2], and *Upf2*$^{wt/wt}$;α*CaMKII*:*CreER*^{T2}(CTRL) or *Upf2*$^{fl/fl}$;α*CaMKII*:*CreER*^{T2} (CKO) adults were used. To induce Cre, mice were treated with 200 mg tamoxifen/kg body weight every other day for five days. To outline dendrites and spines, an AAV-*CaMKIIa-eGFP* virus (Addgene; 50469-AAV5) was injected into the adult hippocampus of CTRL and CKO mice. All animal experiments were completed with the approval of Weill Cornell Medical College ethical committees and per Research Animal Resource Center (RARC) guidelines.

Hippocampal neuronal cultures

For culturing hippocampal neurons, we followed a previously described protocol with some modifications [3]. We typically isolated hippocampal neurons from embryos at embryonic day 16 (E16) and plated 1×10^5 neurons per coverslip (diameter: 12 mm) pre-coated with poly D-lysine (PDL) in Neurobasal medium containing 2% B27, 1 mM sodium pyruvate, 2 mM Glutamax, 30% D-glucose and penicillin (100 units/ml) / streptomycin (100 μg/ml).

Compartmentalized culture in microfluidic devices.

Tripartite microfluidic device was designed and manufactured by the Jeon lab. Microfluidic chambers were prepared in house as previously described [4]. To isolate synaptic regions or to selectively treat the synaptic regions as well as post- or presynaptic cells with either pharmacological agents or sh/siRNAs, hippocampal neurons were cultured in tripartite microfluidic devices. The polymethyldimethylsiloxane (PDMS) devices were fabricated as previously described [4]. These devices have different channels separated by a physical barrier with embedded microgrooves (10 μm wide, 3 μm high). Unlike traditional microfluidic chambers with two channels [5], the tripartite PDMS chamber contains three channels (Figure 3). To access a high number of dendritic synapses, a ‘synaptic’ channel was placed 200 μm from the edge of one channel and 500 μm away from the other. Since the average length of dendrites extending into the microgrooves is less than 300 μm at 21 days in culture (DIV21), the closer “postsynaptic cell channel” allows a large number of dendrites to project from this channel to the new “synaptic” channel. On the other hand, the “presynaptic cell channel” that is located 500 μm away from the new channel ensures that only axons from this channel can extend into the synaptic channel. Fluidic isolation is established across the microgrooves, making it possible to isolate synaptic regions or to selectively treat the synaptic regions as well as post- or presynaptic cells. Reagents applied to synaptic channels were as follows: Cycloheximide (10 μM, Calbiochem), MG132 (10 μM, Sigma), and Leupeptin (10 μM, Sigma). siRNAs were applied to synaptic channels at

different concentrations using 10% NeuroPORTER (Sigma) following manufacturer's instructions.

For microfluidic cultures, we reversibly affixed the tripartite chambers to PDL-coated coverslips (Assistant; 50x24mm; two per coverslip) and then place them in 10 cm dishes. For culturing hippocampal neurons, we followed a previously described protocol with some modifications [3]. We typically isolated hippocampal neurons from embryos at embryonic day 16 and plate $1x10^5$ neurons per coverslip (diameter: 12mm) pre-coated with poly D-lysine (PDL) in Neurobasal medium containing 2% B27, 1 mM sodium pyruvate, 2 mM Glutamax, 30% D-glucose and penicillin (100 units/mL) /streptomycin (100 μg/mL). We plated $8x10^4$ neurons in cell-body channels and maintain these cultures in neuronal medium for up to 21 days. For immunostaining, we fixed neurons inside microfluidic chambers and continued with the staining procedure upon careful removal of chambers.

Immunohistochemistry

Hippocampal neuronal cultures were fixed in 4% paraformaldehyde (PFA)/PBS for 15 min, which was followed by 3 x 10 min washes in PBS. In most experiments, standard immunohistochemistry was performed as previously described [4]. Briefly, samples were incubated overnight in PBS containing 1% Triton X-100, 10% normal goat serum and the relevant dilution of primary antibodies. The following morning, samples were washed with PBS (3 x 10 min) to remove any residual primary antibody. Secondary antibodies were incubated in PBS containing 1% Triton X-100 and 10% normal goat serum for 2 hr. Samples were subsequently washed with PBS (3 x 20 min) and mounted (Vectashield, Vector Laboratories). Primary commercial antibodies included PRKAG3 (rabbit; Thermofisher, PA5-13797), ARC (rabbit; Synaptic Systems, 156002), MAP2 (mouse; Abcam, ab11267), SYNAPSIN 1 (SYN1) (rabbit; Abcam, ab64581), UPF3B (rabbit; Sigma, HPA001882), GFP (chick; Thermofisher, A10262), RFP (rabbit; Thermofisher, R10367), mTOR (mouse; Thermofisher, AHO1232), phospho-mTOR-Ser2448 (rabbit; Cell Signaling #2971), SQSTM1/p62 (mouse; ABCAM, ab56416), NEUN (rabbit; ABCAM, ab177487, GAP-43 (Rabbit; SANTA CRUZ, sc-10786). Two commercial GLUR1 antibodies were used: mouse GLUR1 antibody (Abcam, ab174785) for stainings with SYNAPSIN and rabbit GLUR1 antibody (Calbiochem, pc246) for the internalization assay. Anti-UPF1 and anti-UPF2 antibodies (both rabbit) were a gift from Jens Lykke-Andersen. Secondary antibodies were Alexa 488, 546, and 647 conjugated (Molecular Probes, 1:2000). Immunostaining for PRKAG3 was performed by using a peroxidase-based signal amplification system (Tyramid Signal Amplification, TSA, PerkinElmer) according to manufacturer's instructions. TSA enables much higher dilution of primary antibodies than standard protocols. Higher dilution of primary antibodies reduced nonspecific interactions and improved the specificity of staining.

qRT-PCR, mRNA half-life and siRNA constructs

RNA was isolated from the synaptic channels of microfluidic devices by perfusion with TRIzol reagent (Invitrogen), with RNA being subsequently extracted from lysates following the manufacturer's instructions. Purified RNA was incubated with DNase I (RNase-Free DNase Set, Qiagen) over a mini kit column (RNAeasy, Qiagen) to ensure DNA digestion.

SuperScript III First-Strand Synthesis SuperMix (Invitrogen) was used to amplify cDNAs in a 20 μl reaction using 1 μg of RNA. Quantitative Real-Time PCR (qRT-PCR) reactions were performed as previously described [4] using the iQ SYBR Green Supermix (Bio-Rad) and an Eppendorf Mastercycler EP Realplex Thermocycler. For each reaction 10 ng cDNA was used. Relative expression levels were either normalized to *Gapdh* or *Beta-Actin*. To determine the estimated half-life of *Arc* and *Prkag3* mRNAs, a final concentration of 10 μg/ml actinomycin D was added to control and UPF2-deficient neurons. The RNA was harvested at 0, 1 hr and 2 hr time points, and normalized against baseline measurements at 0 hr. The cDNAs were prepared and qRT-PCR was performed as described above.

Primers used for qRT-PCR:

Arc Primers:

(FW) 5’ GGGTGAGCTGAAGCCACAAAT 3’

(REV) 5’ GAGCTGAGCTCTGCTCTTCTT 3’

Arc Pre-mRNA Primers:

(FW) 5’ GGGTGAGCTGAAGCCACAAAT 3’

(REV) 5’ CTCCACCCTTGCAACTAATTT 3’

Prkag3 primers:

(FW) 5’ CAGGTCTACATGCACTTCATGC 3’

(REV) 5’ AAAGCTCTGCTTCTTGCTGTCC 3’

Prkag3 Pre-mRNA Primers:

(FW) 5’ TGGCCACCAGCTCAGAAAGA 3’

(REV) 5’ GTCAAGCTCTGCTCTGGAATT 3’

GluR1 primers:

(FW) 5’AGAGAAGAGGAGGAGAGCAG 3’

(REV) 5’ CTATCTGGATATTGTTGGGGA 3’

Gapdh primers:

(FW) 5’ ACATGGTCTACATGTTCC 3’

(REV) 5’ CAGATCCACAACGGAATAC 3’

Beta-Actin primers:

(FW) 5’ AGTGTGACGTTGACATCCGT 3’

(REV) 5’ TGCTAGGAGCCAGAGCAGTA 3’

Dicer-substrate siRNAs were acquired from Integrated DNA Technologies, and were predesigned using their proprietary algorithm, which integrates design principles from 21mer siRNA theory with updated 27mer criteria. This design process ensures siRNA target sites do not match known single nucleotide polymorphisms or exons that are the product of alternative splicing, with all sequences having been pre-screened using Smith-Waterman analysis to reduce off-target binding.

Arc siRNA Cocktail

Duplex 1:

5’ CUGAUGGCUAUGACUAUACCGUUAG 3’

3’ UCGACUACCGAUACUGAUAUGGCAAUC 5’

Duplex 2:

5’ CUACAUGGACUGAACAUCAAGAAGC 3’

3’ ACGAUGUACCUGACUUGUAGUUCUUCG 5’

Prkag3 siRNA

5’ GUCAAGAGAUGGACUUCUUAGAACA 3’

3’ GAGUCAAGAGATGGACUUCUUAGAACA 5’

Upf3b siRNA Cocktail

Duplex 1:

5’ AAAUUGAAGCCAAAAAUCGAGAATT 3’

3’ CCUUUAACUUCGGUUUUUAGCUCUUAA 5’

Duplex 2:

5’ GGGUCAAGAAUAUCAUGCUAUAGTA 3’

3’ UUCCCAGUUCUUAUAGUACGAUAUCAU 5’

Fluorescent *in-situ* hybridization (FISH) for *Upf3b* mRNA

For the detection of *Upf3b* mRNA, a mix of five non-overlapping antisense probes were used. Each oligonucleotide was 49 base pairs in length. FISH was visualized using the Tyramide In Situ System (Perkin Elmer) as previously described [4]. Briefly, samples were pretreated with hybridization buffer (50% formaldehyde, 5 x SSC, 0.1% tween, 100 ug/ml tRNA [Roche], 50 ug/ml heparin [Sigma]) for 2 hr at 65°C. Riboprobes were (100 ng/μl) were next heated to 97°C for 7 min and left to cool on ice. Hybridization was performed

overnight at 65°C, and was followed by a series of washes at room temperature in hybridization buffer (no tRNA or heparin, 2 x 30 min), hybridization buffer/PBT (0.1% tween in PBS, 2 x 30 min), and lastly just PBT (4 x 30 min). Samples were next blocked for 1 hr (Roche Blocking Solution) and incubated with anti-DIG-POD (Roche) 1:800 in PBT overnight at 4°C. The following morning, samples were washed in PBT (3 x 20 min). Detection was visualized with tyramide-488 1:50 in supplied amplification buffer from the TSA-Plus *in situ* kit (Perkin Elmer).

Oligonucleotides used for antisense *Upf3b* probes

1- GGAAGAAAAAGATCATAGGCCTAAGGAGAAACGAGTGACCCTGTTTACG

2- GTCAAGAATATCATGCTATAGTAGAATTTGCACCATTTCAAAAAGCTGC

3- AAGAAAAGAGAGAAGAAAGGAGGAGACGGGAAATAGAGAGGAAAAGGCA

4- AAGAAAGAGCCAGTGGGCACAGTTATACTCTGCCCAGGCGTTCTGATGT

5- GGCACTTCGAGATAAAGGAAAGAAGAGTGAGAATACAGAATCAATATGC

Oligonucleotides used for sense *Upf3b* probes

1- ATAGGAGTATACATACGGTCTCGTATATAGTTGAAATTTTTGGTTCTTC

2- GCTTCTAATGGAGGGTGAAACTGGTTCCTTGTCGAAGTCCTTGTAGAAG

3- CCTCTCAATACGGTGTCTGTTACTCTTTTACTGTAGATGAGGTCTCTGT

4- CTTAAGGTCTTTCCCTCTTTTATTCCCTACTTGGTTTCTAATTCAACGA

5- CTAATGTCTCTGTCCCTGGCCCTGATACTCTCTCTAGTCCTCGCGTACT

Oligonucleotides used for antisense *Gapdh* probes

1- GGCTGCCATTTGCAGTGGCAAAGTGGAGATTGTTGCCATCAACGACCCC

2- TTGTCATCAACGGGAAGCCCATCACCATCTTCCAGGAGCGAGACCCCAC

3- GGTGGAGCCAAAAGGGTCATCATCTCCGCCCCTTCTGCCGATGCCCCCA

4- ACCCAGAAGACTGTGGATGGCCCCTCTGGAAAGCTGTGGCGTGATGGCC

5- AAGTATGATGACATCAAGAAGGTGGTGAAGCAGGCATCTGAGGGCCCAC

Oligonucleotides used for sense *Gapdh* probes

1- CAGATGTACAAGGTCATACTGAGGTGAGTGCCGTTTAAGTTGCCGTGTC

2- GCCACGACTCATACAGCACCTCAGATGACCACAGAAGTGGTGGTACCTC

3- CCGGTTCCAGTAGGTACTGTTGAAACCGTAACACCTTCCCGAGTACTGG

4- GTACCGGAAGGCACAAGGATGGGGGTTACACAGGCAGCACCTAGACTGC

5- GTAACGAGAGTTACTGTTGAAACAGTTCGAGTAAAGGACCATACTGTTA

GLUR1 internalization assay

GLUR1 internalization experiments were carried-out and quantified as previously described [6, 7]. Briefly, we incubated live DIV21 hippocampal cultures infected with control or *Upf2* shRNAs at 37°C for 5 min with GLUR1 antibody (Calbiochem, PC246) to allow labeling of surface GLUR1. After washing, we incubated neurons at 37°C for 10 min to allow for basal internalization. We then fixed neurons with 4% PFA in PBS and blocked in a detergent-free blocking solution for 1 hr. Following blocking, we incubated neurons with AlexaFluor546 secondary antibody for 1 hr to label the surface population. To label the pre-labeled internalized fraction, we post-fixed neurons with 100% methanol at −20°C for 1 min and stained with Alexa-647 secondary antibody. We calculated the percent internalization by dividing the integrated far-red intensity (internalized GLUR1) by the total (red + far red) intensity between control and UPF2-deficient neurons.

Click chemistry and SDS-page

To measure the dendritic translation of *GluR1*, we used a click chemistry based approach and labeled locally synthesized GLUR1 at synaptic regions. At DIV21, we exchanged the growth media in the synaptic channels to methionine-free medium containing the methionine-analog azidohomoalanine (AHA; 25 μM) for 6 hr. AHA is incorporated into all newly synthesized proteins. After harvesting the material from the synaptic channels in RIPA, we incubated the lysate with DBCO-biotin [8] (30 μM; Click Chemistry Tools LLC) for 1 hr at ambient temperature. DBCO reacts with AHA [9], functionalizing newly synthesized proteins with biotin. We purified biotin-containing proteins with Dynabeads (150 μl per reaction; Dynabeads M-280 Streptavidin-Thermo Fisher Scientific). Dynabeads were separated over a magnetic rack and subsequently washed 2 times in PBS containing 0.1% Bovine Serum Albumin (BSA). Proteins were dissociated and denatured from beads by boiling Dynabeads for 5 min in 0.1% SDS. Lysates were subsequently analyzed for protein concentration via BCA Protein Assay (Thermofisher). Proteins were separated via SDS-PAGE, as previously described [10]. Briefly, protein aliquots were mixed with an equal volume of loading buffer, denatured at 95°C and loaded onto 8% gels before being subject to SDS-PAGE. Proteins were subsequently transferred to nitrocellulose membrane, incubated in 5% BSA diluted in TBST for 1 hr and then incubated with primary anti-C-terminus GLUR1 antibody overnight (Abcam, ab31232). Membranes were washed in TBST (3 x 5 min), incubated for 1 hr in IRDye 800CW goat anti-rabbit secondary (Licor) diluted in 5% low-fat milk diluted in TBST, and bands resolved on a Licor Odyssey CLx imager.

RNA Co-immunoprecipitation and RT-PCR

DIV7 hippocampal neurons were harvested in RNase-free PBS and quickly frozen in liquid nitrogen. The frozen cells were resuspended in 500 μl of B70 (70 mM KAc, 1 mM NaF, 5 mM MgOAc, 0.1% Triton X-100, 10% glycerol, 50 mM HEPES-KOH, pH 7.4, RNase-free) supplemented with fresh protease and phosphatase inhibitors and homogenized using a motor pestle. After the cell debris was removed by centrifugation, the supernatant was used

for RNA co-immunoprecipitation following a published protocol (4). Briefly, the supernatant was divided into two equal samples, which were precleared on the Dynabeads Protein A (Invitrogen). Ten microliters of aliquot was transferred from each sample and saved as input samples. UPF1 antibody and IgG control were added to the remaining precleared supernatant samples, respectively, and incubated for 1 hr on a rotating wheel. The extract-antibody mixes were then added to the Dynabeads Protein A, which was preblocked with B70 containing 10 mg/ml BSA, 0.1 mg/ml yeast total RNA, and 0.1 mg/ml heparin, and incubated for 1 hr on a wheel. After extensive washing with B70, the immune-complexes on beads were directly used to synthesize the first strand cDNA by the SuperScript III CellsDirect cDNA Synthesis System (Invitrogen). Then 2 μl each of the first strand cDNA was used for a 25 μl PCR reaction. The aforementioned primers for *Arc*, *Prkag3* and *Gapdh* were used for RT-PCR. The PCR conditions were 95°C, 30 s; 57°C, 30 s; 72°C, 30 s; 35 cycles.

Electrophysiology

The electrophysiology experiments were performed as previously described (114). All experiments were performed on transvers hippocampal slices (400 μm) from 3-month old (LTP studies) or 6-week-old (LTD studies) $Upf2^{fl/fl}$;α*CaMKII*:$CreER^{T2}$ mice and their control littermates ($Upf2^{wt/wt}$;α*CaMKII*:$CreER^{T2}$) following induction of Cre expression by tamoxifen (Sigma) at 2-months (for LTP) and 1-month (for LTD) of age. Given that Tamoxifen is fat soluble, we prepared our tamoxifen solution by dissolving the relevant quantity of drug into sunflower oil with 1:10 ETOH added. Tamoxifen solutions were incubated at 37°C with rocking for 6-8 hr. Tamoxifen was administered via oral gavage at 200 mg tamoxifen/kg body weight every other day for five total doses. This tamoxifen regimen led to successful ablation of UPF2 protein in the adult brain (Figure S1a). Slice preparation and aCSF composition were performed as described previously [11, 12]. Briefly, slices were isolated and transferred to recording chambers (preheated to 32°C), where they were superfused with oxygenated aCSF. We recorded field excitatory postsynaptic potentials (fEPSPs) from the stratum radiatum of CA1 using microelectrodes filled with artificial cerebrospinal fluid (ACSF) (resistance 1-4 MΩ). A bipolar Teflon-coated platinum electrode was placed in the stratum radiatum of CA3 to activate Schaffer collateral/commissural afferents at 0.05 Hz. Slices recovered in the recording chamber at least 1 hr before recordings began. In all experiments, basal field excitatory postsynaptic potentials (fEPSPs) were stable for at least 20 min before the start of each experiment. LTP was induced with either one (E-LTP) or three 1 sec 100-Hz high-frequency stimulation (HFS) trains, with an intertrain interval of 60 sec. To induce mGluR-LTD, slices were incubated with DHPG (100 μM) for 10 min. After induction of either E-LTP or mGluR-LTD, we collected fEPSPs for an additional 60 min (180 min for L-LTP). Slope values were compared from the conditional *Upf2* mutant mice and their control littermates.

Stereotaxic injection of virus and hippocampal spine density analysis

To measure hippocampal spine density, the spine density of CA1 hippocampal neurons in control (CTRL: $Upf2^{wt/wt}$;α*CaMKII*:$CreER^{T2}$) and Conditional Knockout (CKO: $Upf2^{fl/fl}$;α*CaMKII*:$CreER^{T2}$) mice was examined post-labelling with GFP-expressing virus. To target the dorsal CA1 field, the stereotaxic coordinates AP: −2, ML: 1.6, DV: 1.5-.25

were used. 1 μl of AAV-*CaMKIIa-eGFP* (Addgene, #50469-AAV5) virus was injected bilaterally using a 10 μl nanofil syringe (World Precision Instruments) fitted with a 33-gauge beveled needle. Post-surgery, wounds were closed with tissue adhesive (Vetbond, 3M). For *in vivo* rescue experiments, equal volumes (50:50) of mCMV>Arc-shRNA:TurboRFP (Dharmacon, #V3SM7598-08EG11838) and mCMV>Prkag3-shRNA:TurboRFP (Dharmacon, #V3SM7598-08EG241113) lentivirus were pooled into a master-mix before injection into the dorsal CA1 field as described above. For all spine experiments, mice were transcardially perfused 7 days later with 4% PFA (without PBS flush), brains removed, and sectioned at 200 μm. Hippocampal dendrites were imaged on an Olympus FluoView-FV1000 confocal microscope. To identify spines, we measured maximal spine head width (W_H), neck width (W_N), and length (L) of spines using ImageJ. Spines were identified as Stubby ($L \leq 1$ μm), Mushroom ($1 < L \leq 3$ μm; $W_H \geq 2 \times W_N$), Long Thin ($1 < L \leq 3$ μm; $W_H < 2 \times W_N$), and Filopodia ($3 < L \leq 5$ μm).

Arc-shRNA Lentiviral Sequence:

TATTCTTCAGAGCCACCCA

Prkag3-shRNA Lentiviral Sequence:

AGGCGCTGAGGGCATCGAT

Behavioral assays

To study the role of NMD in cognitive function, we induced Cre in 2-month old *Upf2* CKO mice as well as in their control littermates by tamoxifen. This experimental design ensured that phenotypes are not caused by an acute effect of tamoxifen, or a non-specific effect of Cre at cryptic LoxP sites. A 2-week washout period followed tamoxifen dosing before behavior began, at approximately 3-months of age. The Y-maze [13, 14], fear conditioning [14, 15], Morris water maze [16, 17], marble burying [18], grooming (12), locomotor hyperactivity/open field [19], elevated-plus maze [19, 20] and three-chamber social interaction assay [21] were completed and analyzed as previously described, except where outlined below. Briefly, the Y-Maze comprised exposing mice to 2 of 3 arms of the maze for 10 min as a training trial. The third, blocked, arm of the maze was designated as the novel arm, and was pseudorandomized between mice. Following a 1 hr delay, mice were returned to the maze but were free to explore all 3 arms for 5 min. The time spent exploring the novel arm, relative to the other familiar arms, was quantified as our index of short-term spatial memory. To examine associative memory, we utilized a simple 2-day fear conditioned memory protocol. On day 1, mice were exposed to a 6 min conditioning trial that involved 3 tone-shock pairings. A 30-sec tone duration and 30 sec ISI was utilized, while all shock stimuli comprised a 0.7mA scrambled foot-shock that co-terminated with tone presentation. Learning was evaluated by plotting % freezing to each successive tone presentation as a time-course. On day 2, mice were returned to their conditioning context for 6 min, with % freezing over the test session being quantified as contextual fear memory. All experiments were completed in Colbourn fear chambers. The Morris water maze was used to test more sophisticated learning and longer-term spatial memory. Learning was measured by training mice to find a hidden platform (four trials per day, 75 sec/trial) over 4 consecutive days of

testing. Trials on each day of testing were averaged, and plotted as a time-course, with gradually decreasing escape latencies being used as our index of spatial learning behavior. To assess spatial memory, we conducted a probe trial 24 hr after the last day of training on day 5. In this trial, the hidden escape platform was removed from the pool. Latency to enter the hidden platform zone, and time spent exploring the target quadrant, were quantified as measurements of spatial memory. Reversal learning was not evaluated as *Upf2* CKO mice did not display adequate learning behavior, thus making it impossible to distinguish a general learning deficit from a reversal learning deficit even with addition of extra training trials. Assays were performed in order of least stressful (locomotor hyperactivity/open field) to most stressful (Morris water maze). Mice were bred and tested across 4-5 small cohorts, ensuring that all phenotypes were independent of idiosyncratic effects or nuisance variability that may contaminate any single day of testing. Where experiments were not scored using automated systems (e.g. marble burying), two experimenters scored task performance and in these cases at least one scorer was blinded.

Data analysis

Where total protein levels were measured via immunostaining, Image J was used to measure total fluorescence. In these analyses, a defined area containing dendrites were identified and the integrated fluorescent density was measured in each region. Background fluorescence was measured by selecting a region adjacent to dendrites, and was subtracted from positive fluorescent signal-measurements to derive corrected total fluorescence. Depending on the test, behavior was analyzed using a between-groups or mixed-model ANOVA with genotype and sex added as main effects. For tests that involved multiple observations, data were corrected using Tukey's method. Consistent with prior research [10, 14, 22], as no significant interaction involving the main effect of sex was observed on any given behavioral assay – explicating no modulatory effect of sex on genotype-dependent effects – data from mice were pooled to increase power. No specific exclusion criteria were applied to the datasets, excepting the removal of outliers (defined as values falling outside of ± 2 S.D.). Significance was set at p=0.05 per Fisher's tables, and datasets did not exhibit gross features requiring transformation to ensure test assumptions. Sampling was conducted to levels adequate to detect large effect sizes depending upon observed power, or to levels consistent with prior technical and/or experimental publications that predetermined these parameters. Both animal and cellular experiments were pseudorandomly selected for treatment allocations. Data analysis was completed using the Graphpad Prism software package.

Supplementary Material

Refer to Web version on PubMed Central for supplementary material.

Acknowledgements

We thank J. Lykke-Andersen for generously providing the anti-UPF1 and anti-UPF2 antibodies, M.E. Ross for helpful comments and suggestions and M. Toth for helpful suggestions regarding behavioral assays. This work was supported by a NHMRC CJ Martin Biomedical Fellowship awarded to M.N., KoreaNRF-2015R1A2A1A09005662 to N.L.J., NIH grants NS034007 and NS047384 to E.K, and NIH R01 MH114888 and Leon Levy Foundation Grants to D.C.

References

1. Doma MK and Parker R, RNA quality control in eukaryotes. Cell, 2007 131(4): p. 660–668. [PubMed: 18022361]
2. Hodgkin J, et al., A new kind of informational suppression in the nematode caenorhabditis elegans. Genetics, 1989 123(2): p. 301–313. [PubMed: 2583479]
3. Leeds P, et al., Gene products that promote mRNA turnover in Saccharomyces cerevisiae. Mol Cell Biol, 1992 12(5): p. 2165–2177. [PubMed: 1569946]
4. Lejeune F and Maquat LE, Mechanistic links between nonsense-mediated mRNA decay and pre-mRNA splicing in mammalian cells. Curr Opin Cell Biol, 2005 17(3): p. 309–15. [PubMed: 15901502]
5. Li S and Wilkinson MF, Nonsense surveillance in lymphocytes? Immunity, 1998 8(2): p. 135–41. [PubMed: 9491995]
6. Maquat LE, et al., Unstable beta-globin mRNA in mRNA-deficient beta o thalassemia. Cell, 1981 27(3 Pt 2): p. 543–53. [PubMed: 6101206]
7. Carter MS, et al., A regulatory mechanism that detects premature nonsense codons in T-cell receptor transcripts in vivo is reversed by protein synthesis inhibitors in vitro. J Biol Chem, 1995 270(48): p. 28995–9003. [PubMed: 7499432]
8. Zhang J, et al., At least one intron is required for the nonsense-mediated decay of triosephosphate isomerase mRNA: a possible link between nuclear splicing and cytoplasmic translation. Mol Cell Biol, 1998 18(9): p. 5272–83. [PubMed: 9710612]
9. Karam R, et al., Regulation of nonsense-mediated mRNA decay: implications for physiology and disease. Biochim Biophys Acta, 2013 1829(6–7): p. 624–33. [PubMed: 23500037]
10. Mendell JT, et al., Nonsense surveillance regulates expression of diverse classes of mammalian transcripts and mutes genomic noise. Nat Genet, 2004 36(10): p. 1073–8. [PubMed: 15448691]
11. Colak D, et al., Regulation of axon guidance by compartmentalized nonsense-mediated mRNA decay. Cell, 2013 153(6): p. 1252–65. [PubMed: 23746841]
12. Rebbapragada I and Lykke-Andersen J, Execution of nonsense-mediated mRNA decay: what defines a substrate? Curr Opin Cell Biol, 2009 21(3): p. 394–402. [PubMed: 19359157]
13. Giorgi C, et al., The EJC factor eIF4AIII modulates synaptic strength and neuronal protein expression. Cell, 2007 130(1): p. 179–91. [PubMed: 17632064]
14. Fujimoto T, et al., Arc interacts with microtubules/microtubule-associated protein 2 and attenuates microtubule-associated protein 2 immunoreactivity in the dendrites. J Neurosci Res, 2004 76(1): p. 51–63. [PubMed: 15048929]
15. Husi H, et al., Proteomic analysis of NMDA receptor-adhesion protein signaling complexes. Nat Neurosci, 2000 3(7): p. 661–9. [PubMed: 10862698]
16. Moga DE, et al., Activity-regulated cytoskeletal-associatedprotein is localized to recently activated excitatory synapses. Neuroscience, 2004 125(1): p. 7–11. [PubMed: 15051140]
17. Rodriguez JJ, et al., Long-term potentiation in the rat dentate gyrus is associated with enhanced Arc/Arg3.1 protein expression in spines, dendrites and glia. Eur J Neurosci, 2005 21(9): p. 2384–96. [PubMed: 15932597]
18. Guzowski JF, et al., Inhibition of activity-dependent arc protein expression in the rat hippocampus impairs the maintenance of long-term potentiation and the consolidation of long-term memory. J Neurosci, 2000 20(11): p. 3993–4001. [PubMed: 10818134]
19. Plath N, et al., Arc/Arg3.1 is essential for the consolidation of synaptic plasticity and memories. Neuron, 2006 52(3): p. 437–44. [PubMed: 17088210]
20. Smith-Hicks C, et al., SRF binding to SRE 6.9 in the Arc promoter is essential for LTD in cultured Purkinje cells. Nat Neurosci, 2010 13(9): p. 1082–9. [PubMed: 20694003]
21. Waung MW, et al., Rapid translation of Arc/Arg3.1 selectively mediates mGluR-dependent LTD through persistent increases in AMPAR endocytosis rate. Neuron, 2008 59(1): p. 84–97. [PubMed: 18614031]
22. Cajigas IJ, et al., The local transcriptome in the synaptic neuropil revealed by deep sequencing and high-resolution imaging. Neuron, 2012 74(3): p. 453–66. [PubMed: 22578497]

23. Brown TC, et al., NMDA receptor-dependent activation of the small GTPase Rab5 drives the removal of synaptic AMPA receptors during hippocampal LTD. Neuron, 2005 45(1): p. 81–94. [PubMed: 15629704]
24. Fu AK, et al., APC(Cdh1) mediates EphA4-dependent downregulation of AMPA receptors in homeostatic plasticity. Nat Neurosci, 2011 14(2): p. 181–9. [PubMed: 21186356]
25. Han Y, et al., AMPK Signaling in the Dorsal Hippocampus Negatively Regulates Contextual Fear Memory Formation. Neuropsychopharmacology, 2016 41(7): p. 1849–64. [PubMed: 26647974]
26. Shepherd JD and Bear MF, New views of Arc, a master regulator of synaptic plasticity. Nat Neurosci, 2011 14(3): p. 279–84. [PubMed: 21278731]
27. Addington AM, et al., A novel frameshift mutation in UPF3B identified in brothers affected with childhood onset schizophrenia and autism spectrum disorders. Mol Psychiatry, 2011 16(3): p. 238–9. [PubMed: 20479756]
28. Laumonnier F, et al., Mutations of the UPF3B gene, which encodes a protein widely expressed in neurons, are associated with nonspecific mental retardation with or without autism. Mol Psychiatry, 2010 15(7): p. 767–76. [PubMed: 19238151]
29. Lynch SA, et al., Broadening the phenotype associated with mutations in UPF3B: two further cases with renal dysplasia and variable developmental delay. Eur J Med Genet, 2012 55(8-9): p. 476–9. [PubMed: 22609145]
30. Tarpey PS, et al., Mutations in UPF3B, a member of the nonsense-mediated mRNA decay complex, cause syndromic and nonsyndromic mental retardation. Nat Genet, 2007 39(9): p. 1127–33. [PubMed: 17704778]
31. Nguyen LS, et al., Contribution of copy number variants involving nonsense-mediated mRNA decay pathway genes to neuro-developmental disorders. Hum Mol Genet, 2013 22(9): p. 1816–25. [PubMed: 23376982]
32. Xu X, et al., Exome sequencing identifies UPF3B as the causative gene for a Chinese non-syndrome mental retardation pedigree. Clin Genet, 2013 83(6): p. 560–4. [PubMed: 22957832]
33. Long AA, et al., The nonsense-mediated decay pathway maintains synapse architecture and synaptic vesicle cycle efficacy. J Cell Sci, 2010 123(19): p. 3303–3315. [PubMed: 20826458]
34. Mooney CM, et al., RNA sequencing of synaptic and cytoplasmic Upf1-bound transcripts supports contribution of nonsense-mediated decay to epileptogenesis. Scientific Reports, 2017 7: p. 41517. [PubMed: 28128343]
35. Huang L, et al., A Upf3b-mutant mouse model with behavioral and neurogenesis defects. Mol Psychiatry, 2018 23(8): p. 1773. [PubMed: 28948974]
36. Karam R and Wilkinson M, A conserved microRNA/NMD regulatory circuit controls gene expression. RNA Biol, 2012 9(1): p. 22–6. [PubMed: 22258150]
37. Malenka RC and Bear MF, LTP and LTD: an embarrassment of riches. Neuron, 2004 44(1): p. 5–21. [PubMed: 15450156]
38. Bhakar AL, Dolen G, and Bear MF, The pathophysiology of fragile X (and what it teaches us about synapses). Annu Rev Neurosci, 2012 35: p. 417–43. [PubMed: 22483044]
39. Crabtree GW and Gogos JA, Synaptic plasticity, neural circuits, and the emerging role of altered short-term information processing in schizophrenia. Front Synaptic Neurosci, 2014 6: p. 28. [PubMed: 25505409]
40. Messaoudi E, et al., Sustained Arc/Arg3.1 synthesis controls long-term potentiation consolidation through regulation of local actin polymerization in the dentate gyrus in vivo. J Neurosci, 2007 27(39): p. 10445–55. [PubMed: 17898216]
41. Bassell GJ and Kelic S, Binding proteins for mRNA localization and local translation, and their dysfunction in genetic neurological disease. Curr Opin Neurobiol, 2004 14(5): p. 574–81. [PubMed: 15464890]
42. Buffington SA, Huang W, and Costa-Mattioli M, Translational control in synaptic plasticity and cognitive dysfunction. Annu Rev Neurosci, 2014 37: p. 17–38. [PubMed: 25032491]
43. Darnell JC and Klann E, The translation of translational control by FMRP: therapeutic targets for FXS. Nat Neurosci, 2013 16(11): p. 1530–6. [PubMed: 23584741]
44. Gkogkas CG, et al., Autism-related deficits via dysregulated eIF4E-dependent translational control. Nature, 2013 493(7432): p. 371–7. [PubMed: 23172145]

45. Kelleher RJ 3rd and Bear MF, The autistic neuron: troubled translation? Cell, 2008 135(3): p. 401–6. [PubMed: 18984149]
46. Liu-Yesucevitz L, et al., Local RNA translation at the synapse and in disease. J Neurosci, 2011 31(45): p. 16086–93. [PubMed: 22072660]
47. Santini E, et al., Exaggerated translation causes synaptic and behavioural aberrations associated with autism. Nature, 2013 493(7432): p. 411–5. [PubMed: 23263185]
48. Huber KM, et al., Dysregulation of Mammalian Target of Rapamycin Signaling in Mouse Models of Autism. J Neurosci, 2015 35(41): p. 13836–42. [PubMed: 26468183]
49. Sidorov MS, Auerbach BD, and Bear MF, Fragile X mental retardation protein and synaptic plasticity. Mol Brain, 2013 6: p. 15. [PubMed: 23566911]
50. Weischenfeldt J, et al., NMD is essential for hematopoietic stem and progenitor cells and for eliminating by-products of programmed DNA rearrangements. Genes Dev, 2008 22(10): p. 1381–96. [PubMed: 18483223]
51. Zheng S, et al., PSD-95 is post-transcriptionally repressed during early neural development by PTBP1 and PTBP2. Nat Neurosci, 2012 15(3): p. 381–8, S1. [PubMed: 22246437]
52. Madisen L, et al., A robust and high-throughput Cre reporting and characterization system for the whole mouse brain. Nat Neurosci, 2010 13(1): p. 133–40. [PubMed: 20023653]
53. Kessels HW and Malinow R, Synaptic AMPA receptor plasticity and behavior. Neuron, 2009 61(3): p. 340–50. [PubMed: 19217372]
54. Korb E and Finkbeiner S, Arc in synaptic plasticity: from gene to behavior. Trends Neurosci, 2011 34(11): p. 591–8. [PubMed: 21963089]
55. Penzes P, et al., Dendritic spine pathology in neuropsychiatric disorders. Nat Neurosci, 2011 14(3): p. 285–93. [PubMed: 21346746]
56. Tang G, et al., Loss of mTOR-dependent macroautophagy causes autistic-like synaptic pruning deficits. Neuron, 2014 83(5): p. 1131–43. [PubMed: 25155956]
57. Le Hir H, Sauliere J, and Wang Z, The exon junction complex as a node of post-transcriptional networks. Nat Rev Mol Cell Biol, 2016 17(1): p. 41–54. [PubMed: 26670016]
58. Ashton-Beaucage D, et al., The exon junction complex controls the splicing of MAPK and other long intron-containing transcripts in Drosophila. Cell, 2010 143(2): p. 251–262. [PubMed: 20946983]
59. Fleming JJ and England PM, AMPA receptors and synaptic plasticity: a chemist's perspective. Nat Chem Biol, 2010 6(2): p. 89–97. [PubMed: 20081822]
60. Anggono V and Huganir RL, Regulation of AMPA receptor trafficking and synaptic plasticity. Curr Opin Neurobiol, 2012 22(3): p. 461–9. [PubMed: 22217700]
61. He F and Jacobson A, Nonsense-Mediated mRNA Decay: Degradation of Defective Transcripts Is Only Part of the Story. Annu Rev Genet, 2015 49: p. 339–66. [PubMed: 26436458]
62. Korb E, et al., Arc in the nucleus regulates PML-dependent GluA1 transcription and homeostatic plasticity. Nat Neurosci, 2013 16(7): p. 874. [PubMed: 23749147]
63. Soulé J, et al., Balancing Arc Synthesis, mRNA Decay, and Proteasomal Degradation MAXIMAL PROTEIN EXPRESSION TRIGGERED BY RAPID EYE MOVEMENT SLEEP-LIKE BURSTS OF MUSCARINIC CHOLINERGIC RECEPTOR STIMULATION. J Biol Chem, 2012 287(26): p. 22354–22366. [PubMed: 22584581]
64. Farris S, et al., Selective localization of arc mRNA in dendrites involves activity- and translation-dependent mRNA degradation. J Neurosci, 2014 34(13): p. 4481–4493. [PubMed: 24671994]
65. Ninomiya K, Ohno M, and Kataoka N, Dendritic transport element of human arc mRNA confers RNA degradation activity in a translation-dependent manner. Genes Cells, 2016 21(11): p. 1263–1269. [PubMed: 27659147]
66. Paolantoni C, et al., Arc 3'UTR splicing leads to dual and antagonistic effects in fine-tuning Arc expression upon BDNF signaling. Front Mol Neurosci, 2018 11: p. 145. [PubMed: 29755318]
67. Steward O, et al., Delayed degradation and impaired dendritic delivery of intron-lacking EGFP-Arc/Arg3. 1 mRNA in EGFP-Arc transgenic mice. Front Mol Neurosci, 2018 10: p. 435. [PubMed: 29445324]

68. Chowdhury S, et al., Arc/Arg3.1 interacts with the endocytic machinery to regulate AMPA receptor trafficking. Neuron, 2006 52(3): p. 445–59. [PubMed: 17088211]
69. Aoto J, et al., Presynaptic neurexin-3 alternative splicing trans-synaptically controls postsynaptic AMPA receptor trafficking. Cell, 2013 154(1): p. 75–88. [PubMed: 23827676]
70. Rial Verde EM, et al., Increased expression of the immediate-early gene arc/arg3.1 reduces AMPA receptor-mediated synaptic transmission. Neuron, 2006 52(3): p. 461–74. [PubMed: 17088212]
71. Ju W, et al., Activity-dependent regulation of dendritic synthesis and trafficking of AMPA receptors. Nat Neurosci, 2004 7(3): p. 244–53. [PubMed: 14770185]
72. Lin A, et al., Nedd4-mediated AMPA receptor ubiquitination regulates receptor turnover and trafficking. J Neurochem, 2011 119(1): p. 27–39. [PubMed: 21338354]
73. Schwarz LA, Hall BJ, and Patrick GN, Activity-dependent ubiquitination of GluA1 mediates a distinct AMPA receptor endocytosis and sorting pathway. J Neurosci, 2010 30(49): p. 16718–29. [PubMed: 21148011]
74. Taylor AM, et al., A microfluidic culture platform for CNS axonal injury, regeneration and transport. Nat Methods, 2005 2(8): p. 599–605. [PubMed: 16094385]
75. Ehlers MD, Reinsertion or degradation of AMPA receptors determined by activity-dependent endocytic sorting. Neuron, 2000 28(2): p. 511–25. [PubMed: 11144360]
76. Patrick GN, et al., Ubiquitin-mediated proteasome activity is required for agonist-induced endocytosis of GluRs. Curr Biol, 2003 13(23): p. 2073–81. [PubMed: 14653997]
77. Widagdo J, et al., Activity-Dependent Ubiquitination of GluA1 and GluA2 Regulates AMPA Receptor Intracellular Sorting and Degradation. Cell Rep, 2015.
78. Zhang D, et al., Na,K-ATPase activity regulates AMPA receptor turnover through proteasome-mediated proteolysis. J Neurosci, 2009 29(14): p. 4498–511. [PubMed: 19357275]
79. Dieterich DC, et al., Selective identification of newly synthesized proteins in mammalian cells using bioorthogonal noncanonical amino acid tagging (BONCAT). Proc Natl Acad Sci U S A, 2006 103(25): p. 9482–7. [PubMed: 16769897]
80. Ishigaki Y, et al., Evidence for a pioneer round of mRNA translation: mRNAs subject to nonsense-mediated decay in mammalian cells are bound by CBP80 and CBP20. Cell, 2001 106(5): p. 607–17. [PubMed: 11551508]
81. Singh G, et al., Communication with the exon-junction complex and activation of nonsense-mediated decay by human Upf proteins occur in the cytoplasm. Mol Cell, 2007 27(5): p. 780–92. [PubMed: 17803942]
82. Chamieh H, et al., NMD factors UPF2 and UPF3 bridge UPF1 to the exon junction complex and stimulate its RNA helicase activity. Nat Struct Mol Biol, 2008 15(1): p. 85–93. [PubMed: 18066079]
83. Huang L, et al., RNA homeostasis governed by cell type-specific and branched feedback loops acting on NMD. Mol Cell, 201143(6): p. 950–61. [PubMed: 21925383]
84. Deglincerti A and Jaffrey SR, Insights into the roles of local translation from the axonal transcriptome. Open Biol, 2012 2(6): p. 120079. [PubMed: 22773949]
85. Gumy LF, et al., Transcriptome analysis of embryonic and adult sensory axons reveals changes in mRNA repertoire localization. RNA, 2011 17(1): p. 85–98. [PubMed: 21098654]
86. Taylor AM, et al., Axonal mRNA in uninjured and regenerating cortical mammalian axons. J Neurosci, 2009 29(15): p. 4697–707. [PubMed: 19369540]
87. Jolly LA, et al., The UPF3B gene, implicated in intellectual disability, autism, ADHD and childhood onset schizophrenia regulates neural progenitor cell behaviour and neuronal outgrowth. Hum Mol Genet, 2013 22(23): p. 4673–4687. [PubMed: 23821644]
88. Chan WK, et al., An alternative branch of the nonsense-mediated decay pathway. EMBO J, 2007 26(7): p. 1820–1830. [PubMed: 17363904]
89. Karam R, et al., The unfolded protein response is shaped by the NMD pathway. EMBO Rep, 2015: p. e201439696.
90. Gwinn DM, et al., AMPK phosphorylation of raptor mediates a metabolic checkpoint. Mol Cell, 2008 30(2): p. 214–226. [PubMed: 18439900]

91. Bolster DR, et al., AMP-activated protein kinase suppresses protein synthesis in rat skeletal muscle through down-regulated mammalian target of rapamycin (mTOR) signaling. J Biol Chem, 2002 277(27): p. 23977–23980. [PubMed: 11997383]

92. Inoki K, Zhu T, and Guan K-L, TSC2 mediates cellular energy response to control cell growth and survival. Cell, 2003 115(5): p. 577–590. [PubMed: 14651849]

93. Horman S, et al., Activation of AMP-activated protein kinase leads to the phosphorylation of elongation factor 2 and an inhibition of protein synthesis. Curr Biol, 2002 12(16): p. 1419–1423. [PubMed: 12194824]

94. Kimura N, et al., A possible linkage between AMP-activated protein kinase (AMPK) and mammalian target of rapamycin (mTOR) signalling pathway. Genes Cells, 2003 8(1): p. 65–79. [PubMed: 12558800]

95. Sarbassov DD, Ali SM, and Sabatini DM, Growing roles for the mTOR pathway. Curr Opin Cell Biol, 2005 17(6): p. 596–603. [PubMed: 16226444]

96. Ma T, et al., Inhibition of AMP-activated protein kinase signaling alleviates impairments in hippocampal synaptic plasticity induced by amyloid β. J Neurosci, 2014 34(36): p. 12230–12238. [PubMed: 25186765]

97. Matsuo N, Reijmers L, and Mayford M, Spine-type-specific recruitment of newly synthesized AMPA receptors with learning. Science, 2008 319(5866): p. 1104–1107. [PubMed: 18292343]

98. Whitlock JR, et al., Learning induces long-term potentiation in the hippocampus. Science, 2006 313(5790): p. 1093–1097. [PubMed: 16931756]

99. Reisel D, et al., Spatial memory dissociations in mice lacking GluR1. Nat Neurosci, 2002 5(9): p. 868–73. [PubMed: 12195431]

100. Moretti P, et al., Learning and memory and synaptic plasticity are impaired in a mouse model of Rett syndrome. J Neurosci, 2006 26(1): p. 319–327. [PubMed: 16399702]

101. Swanger SA, et al., Dendritic GluN2A synthesis mediates activity-induced NMDA receptor insertion. J Neurosci, 2013 33(20): p. 8898–8908. [PubMed: 23678131]

102. Farris S, et al., Selective localization of arc mRNA in dendrites involves activity- and translation-dependent mRNA degradation. J Neurosci, 2014 34(13): p. 4481–93. [PubMed: 24671994]

References for Methods

1. Weischenfeldt J, et al., NMD is essential for hematopoietic stem and progenitor cells and for eliminating by-products of programmed DNA rearrangements. Genes Dev, 2008 22(10): p. 1381–96. [PubMed: 18483223]

2. Madisen L, et al., A robust and high-throughput Cre reporting and characterization system for the whole mouse brain. Nat Neurosci, 2010 13(1): p. 133–40. [PubMed: 20023653]

3. Kim Y, et al., Phosphorylation of WAVE1 regulates actin polymerization and dendritic spine morphology. Nature, 2006 442(7104): p. 814–7. [PubMed: 16862120]

4. Colak D, et al., Regulation of axon guidance by compartmentalized nonsense-mediated mRNA decay. Cell, 2013 153(6): p. 1252–65. [PubMed: 23746841]

5. Taylor AM, et al., A microfluidic culture platform for CNS axonal injury, regeneration and transport. Nat Methods, 2005 2(8): p. 599–605. [PubMed: 16094385]

6. Aoto J, et al., Presynaptic neurexin-3 alternative splicing trans-synaptically controls postsynaptic AMPA receptor trafficking. Cell, 2013 154(1): p. 75–88. [PubMed: 23827676]

7. Lin JW, et al., Distinct molecular mechanisms and divergent endocytotic pathways of AMPA receptor internalization. Nat Neurosci, 2000 3: p. 1282–1290. [PubMed: 11100149]

8. Ning X, et al., Visualizing metabolically labeled glycoconjugates of living cells by copper-free and fast huisgen cycloadditions. Angew Chem Int Ed Engl, 2008 47(12): p. 2253–5. [PubMed: 18275058]

9. Agard NJ, Prescher JA, and Bertozzi CR, A strain-promoted [3 + 2] azide-alkyne cycloaddition for covalent modification of biomolecules in living systems. J Am Chem Soc, 2004 126(46): p. 15046–7. [PubMed: 15547999]

10. Notaras M, et al., The BDNF Val66Met polymorphism regulates glucocorticoid-induced corticohippocampal remodeling and behavioral despair. Transl Psychiatry, 2017: p. e1233. [PubMed: 28926000]
11. Trinh MA, et al., The eIF2a kinase PERK limits the expression of hippocampal metabotropic glutamate receptor-dependent long-term depression. Learn Mem, 2014 21: p. 298–304. [PubMed: 24741110]
12. Sharma A, et al., Dysregulation of mTOR signaling in fragile x syndrome. J Neurosci, 2010 30(2): p. 694–702. [PubMed: 20071534]
13. Sarnyai Z, et al., Impaired hippocampal-dependent learning and functional abnormalities in the hippocampus in mice lacking serotonin(1A) receptors. Proc Natl Acad Sci U S A, 2000 97(26): p. 14731–6. [PubMed: 11121072]
14. Notaras M, et al., BDNF Val66Met genotype determines hippocampus-dependent behavior via sensitivity to glucocorticoid signaling. Mol Psychiatry, 2016 21(6): p. 730–732. [PubMed: 26821977]
15. Chen ZY, et al., Genetic variant BDNF (Val66Met) polymorphism alters anxiety-related behavior. Science, 2006 314(5796): p. 140–3. [PubMed: 17023662]
16. Dumont M, et al., Reduction of oxidative stress, amyloid deposition, and memory deficit by manganese superoxide dismutase overexpression in a transgenic mouse model of Alzheimer's disease. FASEB J, 2009 23(8): p. 2459–66. [PubMed: 19346295]
17. Santini E, et al., Exaggerated translation causes synaptic and behavioural aberrations associated with autism. Nature, 2013 493(7432): p. 411–5. [PubMed: 23263185]
18. Angoa-Perez M, et al., Marble burying and nestlet shredding as tests of repetitive, compulsive-like behaviors in mice. J Vis Exp, 2013 82: p. 50978.
19. Mitchell E, et al., Behavioural traits propagate across generations via segregated iterative-somatic and gametic epigentic mechanisms. Nat Commun, 2016 7: p. 11492. [PubMed: 27173585]
20. Walf AA and Frye CA, The use of the elevated plus maze as an assay of anxiety-related behavior in rodents. Nat Protocol, 2007 2: p. 322–328.
21. Moy SS, et al., Sociability and preference for social novelty in five inbred strains: an approach to assess autistic-like behavior in mice. Genes Brain Behav, 2004 3(5): p. 287–302. [PubMed: 15344922]
22. Notaras M, et al., BDNF Val66Met genotype interacts with a history of simulated stress exposure to regulate sensorimotor gating and startle reactivity. Scz Bull, 2017 43(3): p. 665–672.

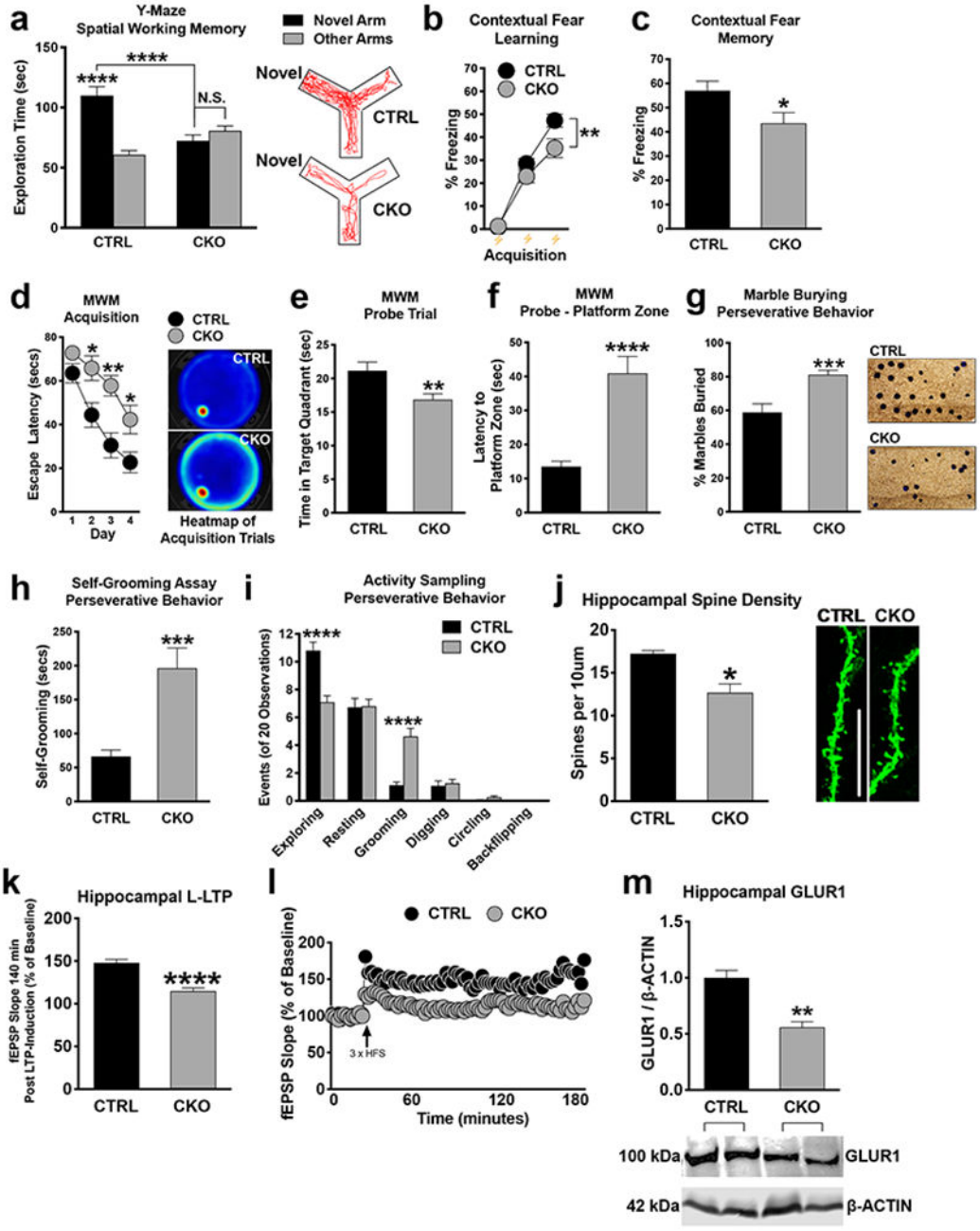

Figure 1. UPF2 is required for learning, memory, spine density, and LTP.

a-c, Impaired short-term spatial and contextual fear memory in CKO mice. Quantitations for relative arm preference on the Y-Maze (n=24 CTRL and 22 CKO mice), freezing during contextual fear conditioning (n = 22 per group, **b)** and freezing during context re-exposure (n = 22 per group, **c**).

d-f, CKO mice exhibit disrupted hippocampus-dependent spatial acquisition. In the MWM, CKO mice exhibited significantly delayed escape latencies on days 2, 3, and 4 compared to CTRL mice (n=18 for each group) (**d**). During the probe trial, CKO spent

significantly less time exploring the target quadrant and took significantly longer to enter the platform zone compared to CTRL mice (n=18 for each group; **f**).

g-i, Increased repetitive and compulsive-like behavior in CKO mice.

CKO mice buried significantly more marbles (n=25 per group) as well as exhibited increased grooming relative to CTRL mice without evidence of further compulsive-like traits (**i**).

j-l, Disrupted hippocampal spine density and synaptic plasticity in CKO mice.

Spine quantification (n=3 mice per group; 4-10 independent apical dendrite; **j**) and LTP measurements (n=12 slices, 7 CTRL mice: n=14 slices, 8 CKO mice) (**k** and **l**) in CTRL and CKO mice.

m, Disrupted GLUR1 expression in the CKO hippocampus.

Western blot of total hippocampal GLUR1 revealed significantly decreased GLUR1 expression in CKO relative to CTRL mice (n= 3 CTRL and 5 CKO mice).

Data are represented as mean ± SEM; *p < 0.05, **p < 0.01, ***p <0.001 and ****p < 0.0001. N.S. represents “Not Significant”. Scale bar: 5 μm.

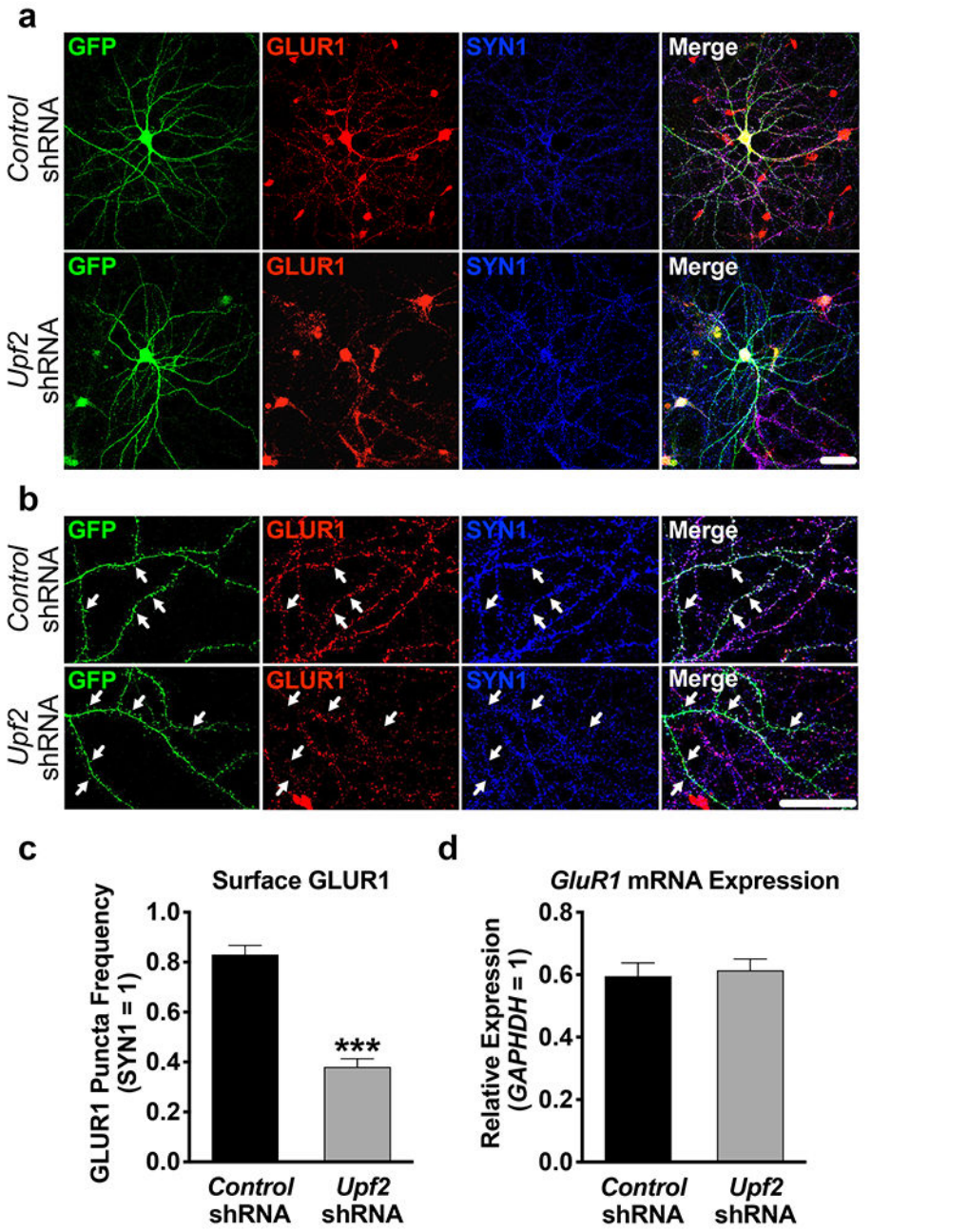

Figure 2. UPF2 is required for surface expression of GLUR1 on dendrites.

a-b, Hippocampal neurons were infected at DIV7 with *control*- or *Upf2-shRNA* lentivirus and fixed at DIV21. Surface GLUR1 expression was detected using an anti-N-terminus-GluR1 antibody (see Methods). Arrows indicate positive and negative GLUR1 signal at spines.

c, UPF2 positively regulates surface GLUR1 levels.

Quantifications of surface GLUR1 frequency in dendrites (n=3/group; 10 neurons-24 dendrites/group). Knockdown of *Upf2* did not change SYN1 density (see Figure S4 for PSD-95 staining) indicating unaltered synaptic potential.

d, Knockdown of *Upf2* does not alter *GluR1* mRNA levels.

qRT-PCR of *GluR1* mRNA levels in *control*- and *Upf2*-shRNA infected neurons (n=3/group; see Figure S7 for infection efficiency).
Data are represented as mean ± (SEM); ***p < 0.001. Scale bar: 20 μm.

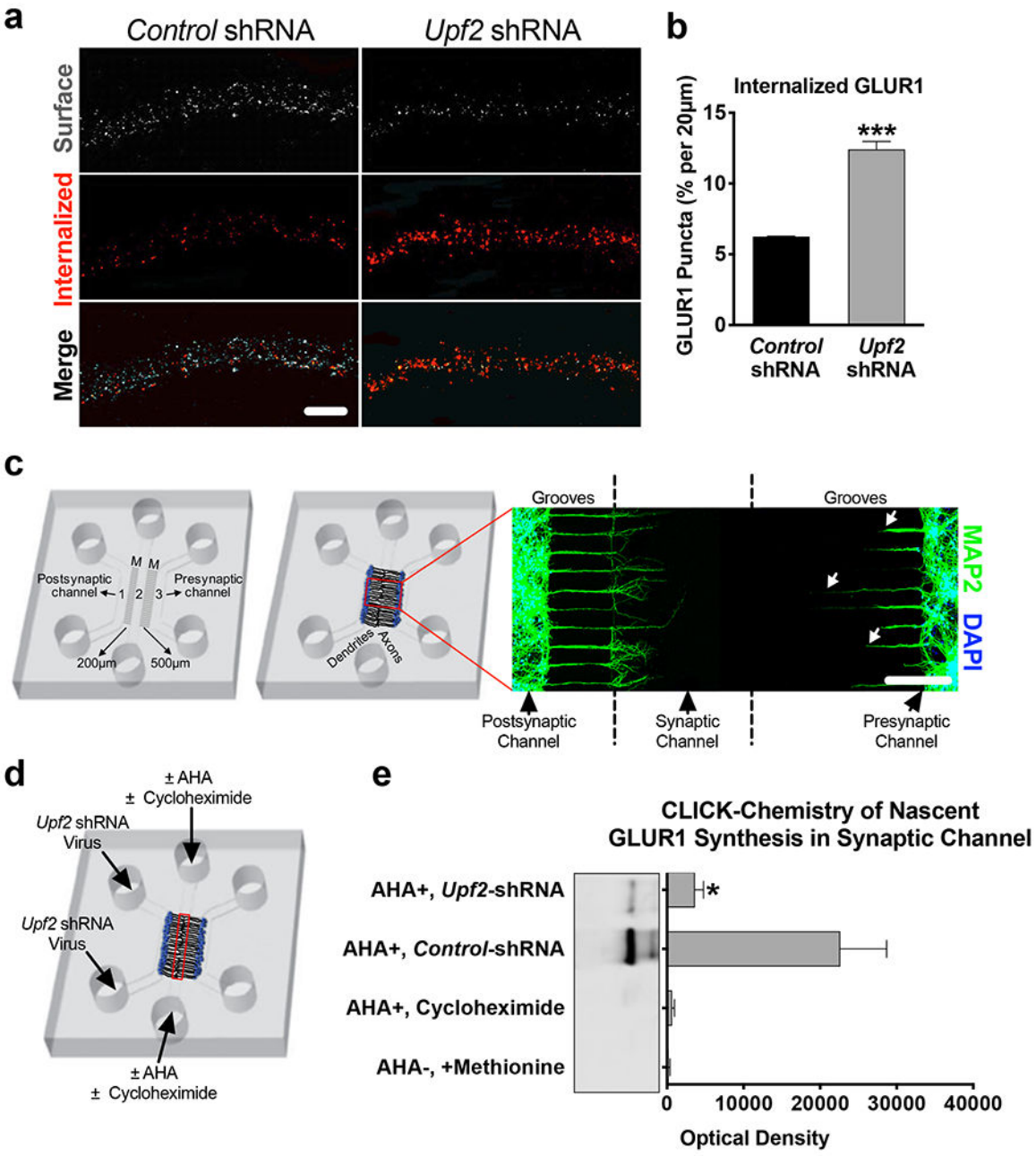

Figure 3. UPF2 regulates GLUR1 internalization and local synthesis in dendrites.

a-b, Increased rates of GLUR1 internalization in UPF2-deficient dendrites.

Basal internalization rates (for 10 minutes) of GLUR1 receptors was achieved by live-staining neurons using anti-N-terminus GLUR1 antibody at DIV 21 (see Methods) (n=3 per *control*-shRNA [13 neurons, 33 dendrites] and per *Upf2*-shRNA [20 neurons, 53 dendrites]).

c, Custom tripartite microfluidic device for compartmentalized synapse access.

In this customized tripartite chamber, the different microgroove (M) lengths between channels created a postsynaptic neuron channel, a presynaptic neuron channel, and a synaptic channel, which enabled selective treatment of these compartments (see Methods). By DIV8, the synaptic channel is exclusively populated with dendrites (MAP2) emerging

from the postsynaptic channel. Arrows highlight that dendrites from the presynaptic channel do not reach the synaptic channel.

d-e, Decreased local synthesis of GLUR1 in UPF2-deficient dendrites.

We cultured E16 hippocampal neurons in tripartite chambers and applied *control*- or *Upf2*-shRNA virus only to postsynaptic neurons at DIV7. The media was exchanged to methionine-free media containing the methionine analog azidohomoalanine (AHA, 25 μM). After harvesting material from the synaptic channels (red box), the proteins were separated by SDS-PAGE, and nascent GLUR1 was detected with an anti-C-terminus antibody (see also Methods).

Data are represented as mean ± SEM; *p < 0.05 and ***p < 0.001. Scale bar: **a** 20 μm, **c** 200 μm.

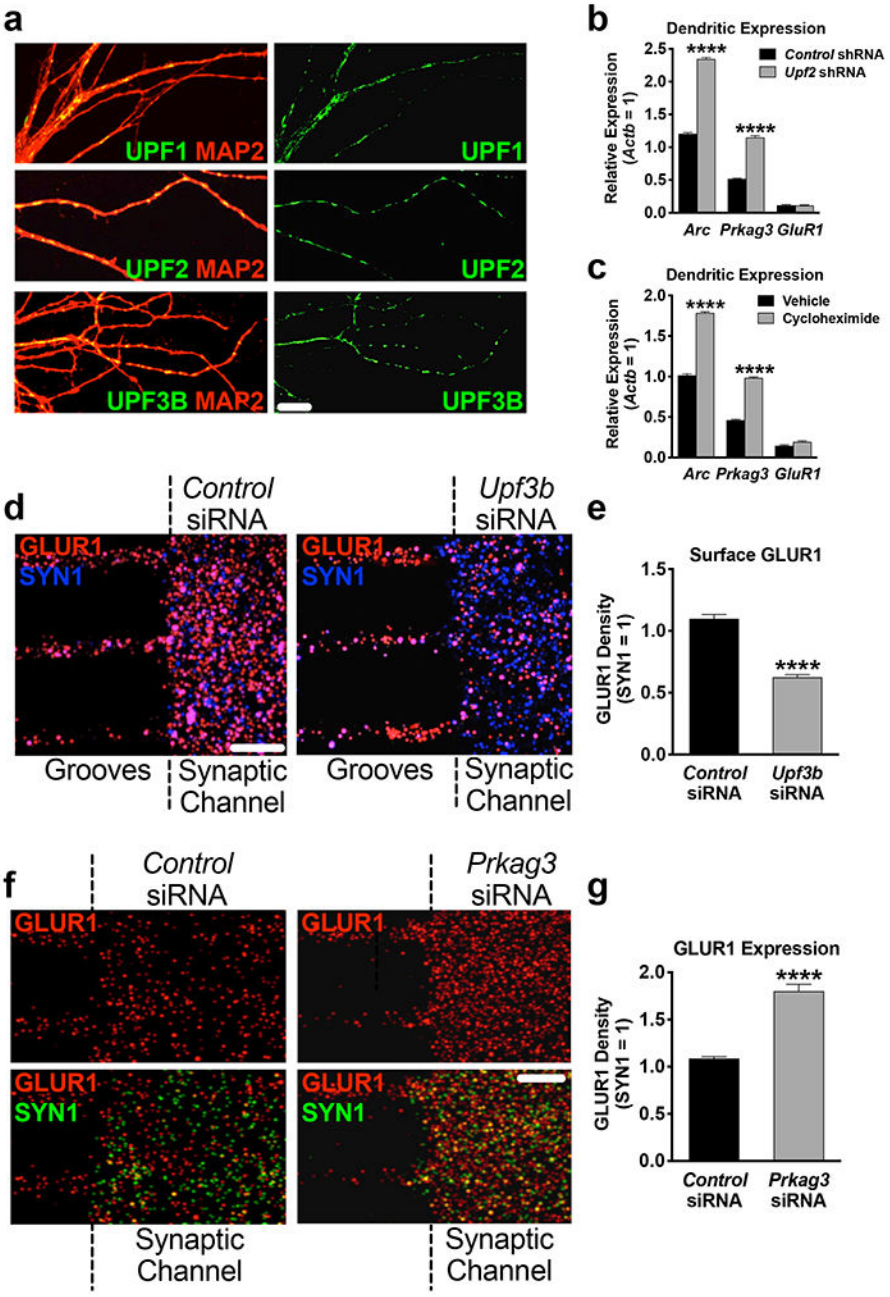

Figure 4. Establishing local regulation of GLUR1 by NMD in dendrites.

a, The NMD machinery is localized to dendrites.

UPF1, UPF2 and UPF3B immunostainings in hippocampal dendrites at DIV7.

b, *Arc* and *Prkag3* mRNAs are increased in UPF2-deficient dendrites.

Synaptic material was harvested from tripartite chambers containing postsynaptic neurons infected with either *control*- or *Upf2*-shRNA virus (n=3) and qRT-PCR for *Arc* and *Prkag3* mRNAs was performed.

c, *Arc* and *Prkag3* mRNAs are subjected to translation-dependent degradation in dendrites. Selective treatment of synaptic channels with the translation inhibitor CHX (10 μM) at DIV21 for 3 hr and qRT-PCR for *Arc* and *Prkag3* mRNAs (n=3).
d, NMD locally regulates surface expression of GLUR1 in dendrites. Repetitive treatment of synaptic channels with non-overlapping *Upf3b*-siRNAs (10 nM) for 7 days led to complete loss of UPF3B protein (Figure S9d) and a >40% decrease in surface GLUR1 compared to control cultures (10 neurons, 10 dendrites per group).
e, Locally synthesized PRKAG3 negatively regulates GLUR1 levels in dendrites. Quantifications of total GLUR1 levels following non-overlapping *Prkag3* siRNA treatment of synaptic channels for 7d (n=3 per *control*-siRNA [6 neurons, 9 dendrites] and per *Prkag3*-siRNA [8 neurons, 9 dendrites]).
Data are represented as mean ± SEM; ****$p < 0.0001$. Scale bar: 30 μm.

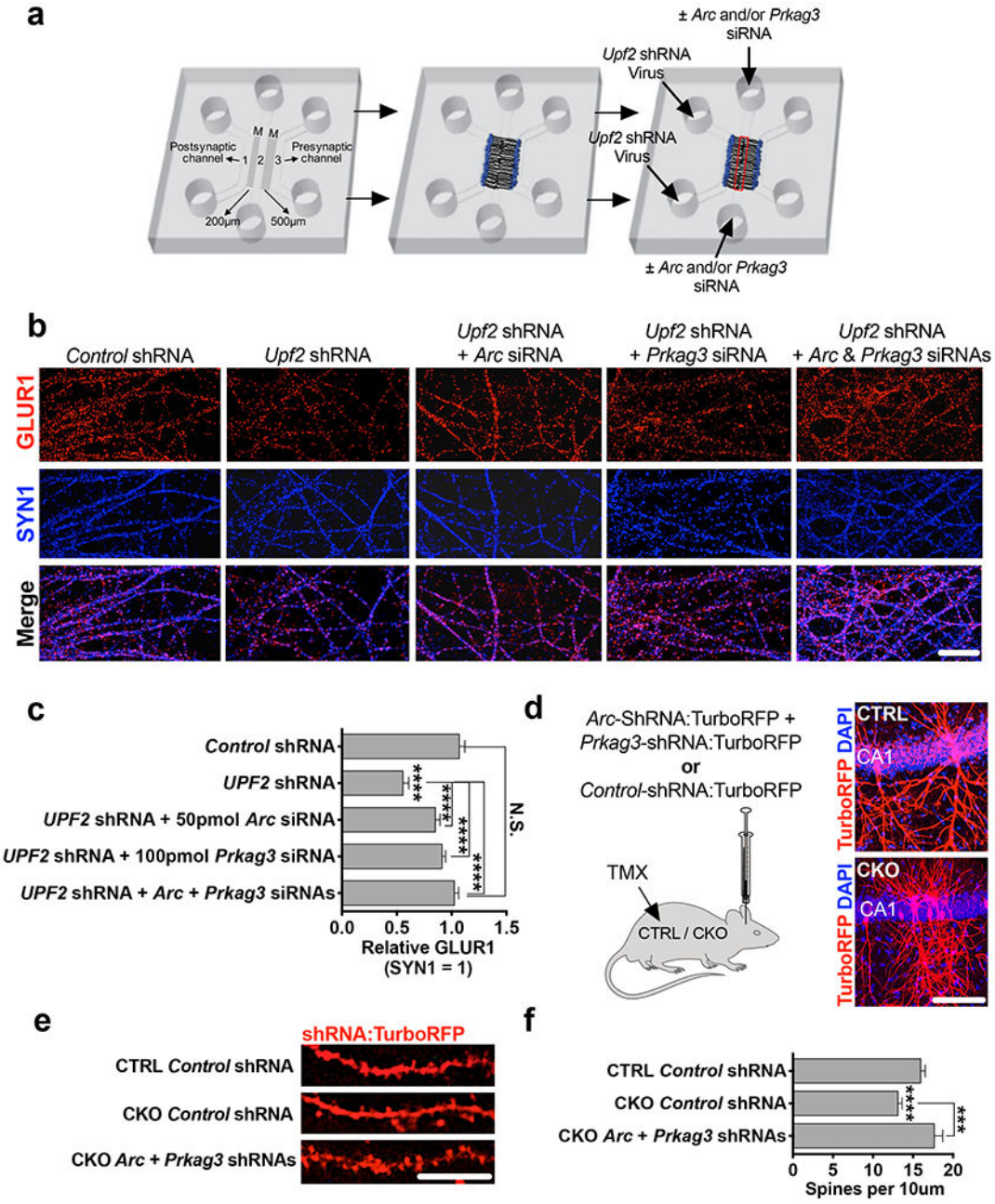

Figure 5. UPF2 mechanistically regulates surface GLUR1 levels and spine density via degradation of *Arc* and *Prkag3* in dendrites.

a-c, Modulating *Arc* and *Prkag3* levels in UPF2-deficient dendrites rescues surface GLUR1. Schematic of the experimental design (**a**; see Figure S11 for knockdown validation) and immunostainings for surface GLUR1 in dendrites upon treatment of UPF2-deficient dendrites with *Arc* and *Prkag3* siRNAs (**b**). siRNA transfection of synaptic channels started at DIV14 and lasted for a week. Quantifications of surface GLUR1 density following normalization of each target (n=3 per *control*-siRNA [10 neurons, 10 dendrites], *Arc*-siRNA [10 neurons, 10 dendrites] and *Prkag3*-siRNA [10 neurons, 10 dendrites]) (**c**).

d-f, Modulating *Arc* and *Prkag3* levels *in vivo* rescues hippocampal spine density. Mice were stereotaxically injected with mCMV>*Arc*-shRNA:TurboRFP and mCMV>*Prkag3*-shRNA:TurboRFP lentiviruses to the dorsal CA1 region of the hippocampus (see Figure S13 for shRNA knockdown validation) (**d**). Representative images (**e**) and quantifications (**f**) of spine density from virus-injected mice (n=3 mice per group [n=14 CTRL + *Control* shRNA dendrite segments, n=22 CKO + *Control* shRNA dendrite segments, and n=16 CKO + *Arc* + *Prkag3* shRNA dendrite segments]).

Data are represented as mean ± SEM; ****p < 0.0001, N.S. represents “Not Significant”. Scale bar: **b** 75 μm, **d** 100 μm, **e** 5 μm.